Vibration and rotation of CO in C_{60} and predicted infrared spectrum

E. H. T. Olthof, A. van der Avoird, and P. E. S. Wormer
Institute of Theoretical Chemistry, NSR-Center, University of Nijmegen, Toernooiveld, 6525 ED Nijmegen, The Netherlands

(Received 31 August 1995; accepted 12 October 1995)

We present the Hamiltonian for the vibrations and rotations of CO inside a freely rotating or fixed C_{60} molecule and we calculate its eigenstates from an atom–atom model potential. The ensuing level structure can be understood in terms of three basic characteristics. (i) Simultaneous rotations of CO and its position vector **R**, which give rise to a rotational structure similar to that of free CO. The effective rotational constants differ considerably, however. (ii) Splittings of the levels by the icosahedral field of C_{60} which perturb the regular rotational structure, because they are of the same order of magnitude as the rotational spacings. (iii) Large frequencies associated with the (nearly harmonic) vibrations of CO against the hard walls of the C_{60} cage: 209 cm^{-1} for the radial excitation and 162 cm^{-1} for the twofold degenerate libration. These vibrations give a rovibrational level structure similar to that of a linear triatomic molecule, the radial excitation resembles a bond stretch (Σ) state, the libration a Π-bending state. From the eigenstates we calculate the line strengths of the electric dipole transitions allowed by the icosahedral symmetry. Additional (approximate) selection rules are found, and the infrared spectrum of $CO@C_{60}$ is predicted.
 [S0021-9606(96)03203-9]

I. INTRODUCTION

The main focus in the research on C_{60}, also called buckyball,[1] has shifted away from the chemistry and physics of the molecule itself and now concentrates on the cavity inside C_{60}. Especially the fact that there is experimental[2–9] and theoretical[10–12] evidence that atoms and even small molecules like H_2, CO, CH_4 can form stable endohedral complexes with C_{60} triggered many research groups to start investigating such complexes. For example the endohedral complexes of C_{60} with He, Ne, Ar, Ca, La, and other atoms have been observed.[2–9] It has become customary to denote such complexes as $X@C_{60}$, where X is the atom or molecule inside C_{60}. In one of the theoretical studies[10] it was shown that CO is one of the molecules that could form a stable endohedral complex with C_{60}. Scientists in the Department of Molecular and Laser Physics of the University of Nijmegen started a research program aimed at the production of $CO@C_{60}$.[4]

In this paper we present quantum mechanical calculations of the dynamics of CO inside C_{60}. Such calculations have been performed earlier[13–15] for rare gas atoms inside fullerenes, but not yet for molecules. Our calculations are similar to those of Liu *et al.*[16,17] for HF molecules trapped in Ar_n cages, although we use a method that is somewhat different from theirs. We have to realize that the complex $CO@C_{60}$ can exist in two forms. In the first place $CO@C_{60}$ can exist as a complex in free space, e.g., in a molecular beam. The second possible form is that of $CO@C_{60}$ diluted in bulk C_{60}. In the production of $CO@C_{60}$ the Nijmegen physicists aim at a mixture of 1% $CO@C_{60}$ in solid C_{60}. In this latter arrangement C_{60} is fixed and the dynamics of CO will be determined by the external potential provided by the presence of the C_{60} cage and environment, although this latter effect is assumed to be small. The peak positions and line strengths calculated in the present paper will help to interpret the measurements. On the other hand, the measurements will provide data that enable us to improve the model potential that we have used.

This paper is organized as follows: Sec. II describes the theory used in this work, which is an extension of a formalism given earlier.[18] In Sec. III the symmetry of C_{60} and the implications of symmetry on the calculations is discussed. In Sec. IV the results of the calculations are presented and discussed. The conclusions are summarized in Sec. V.

II. THEORY

The C_{60} molecule has some rather soft modes, starting at 273 cm^{-1},[19] which might couple with some of the van der Waals modes of the complex. In view of the exploratory nature of the present work, we decided to neglect this coupling and to consider in first approximation C_{60} as a rigid molecule. When constraints such as constant bond lengths and constant angles are introduced, the proper way to obtain the kinetic energy operator is by considering first the corresponding classical problem. Therefore, we will start this section by deriving the classical Hamilton function and then we will quantize, i.e., we will replace the momenta by differential operators (times $-i\hbar$). Although we kept also the CO bond length r fixed in the actual computations, it will be convenient to consider first the case where r is variable. We thus obtain a general expression in which the kinetic energies of the rigid C_{60} and the rovibrating CO are fully taken into account. We will then point out which terms in the kinetic energy must be dropped (i) if C_{60} does not rotate, as is the

 0021-9606/96/104(3)/832/16/$6.00

case in solid C_{60}, and (ii) if CO is kept rigid. We will end this section by presenting formulas for the intensities of infrared transitions.

A. Kinetic energy

All coordinates will be expressed with respect to a rotating coordinate frame, with the orientation of its axes $\{\vec{f}_\alpha\}$ ($\alpha=x,y,z$) parallel to a frame fixed on the fullerene molecule. An obvious choice of the fullerene frame is a principal axes frame, but since C_{60} (frozen in I_h symmetry) is a spherical top, any right-handed frame will do. We choose the C_{60} axes along three orthogonal twofold rotation axes, so that the three coordinate planes are mirror planes. The dimer frame origin is in the center of mass of the complex. The classical kinetic energy of a dimer $A-B$ (A is C_{60}, B is CO) has the following form

$$T=T_A+T_B+T_{AB}, \tag{1}$$

where T_X is the kinetic energy of monomer X, $X=A$ or B, and T_{AB} is the kinetic energy of the "reduced particle." The rotor kinetic energy T_A is given by the well-known expression

$$2T_A=\omega^T\mathbb{I}\omega, \tag{2}$$

where $\boldsymbol{\omega}$ is the angular velocity of A. Note parenthetically that we will not use the fact that the inertia tensor $\mathbb{I}$ is a scalar times the 3×3 unit matrix $\mathbb{E}$, but rather keep the discussion general, so as to apply to any rigid rotor. From standard classical mechanics we know that T_{AB} is given by

$$2T_{AB}=\mu_{AB}|\boldsymbol{\omega}\times\boldsymbol{R}+\dot{\boldsymbol{R}}|^2 \quad \text{with} \quad \mu_{AB}=\frac{m_Am_B}{(m_A+m_B)}. \tag{3}$$

Here m_X is the mass of X and the vector $\boldsymbol{R}$ points from the center of mass of A to the center of mass of B. The kinetic energy of the diatom is

$$2T_B=\mu_{CO}|\boldsymbol{\omega}\times\boldsymbol{r}+\dot{\boldsymbol{r}}|^2 \quad \text{with} \quad \mu_{CO}=\frac{m_Om_C}{(m_O+m_C)}. \tag{4}$$

The vector $\boldsymbol{r}$ points from O (with mass m_O) to C (mass m_C).

A metric tensor $g_{\mu\nu}$ associated with generalized coordinates q_μ may be defined by the following expression

$$2T=\sum_{\mu\nu} g_{\mu\nu}\dot{q}_\mu\dot{q}_\nu. \tag{5}$$

In order to obtain this metric tensor, we must cast Eqs. (1)–(4) into the form of Eq. (5). To that end we will write the vector product as follows:

$$\boldsymbol{\omega}\times\boldsymbol{r}=\mathbb{X}_r^T\boldsymbol{\omega}\equiv\begin{pmatrix}0&z&-y\\-z&0&x\\y&-x&0\end{pmatrix}\boldsymbol{\omega}. \tag{6}$$

In the same way we write $\boldsymbol{\omega}\times\boldsymbol{R}=\mathbb{X}_R^T\boldsymbol{\omega}$. It is apparent now that the total kinetic energy of the dimer can be written in the following form

$$\begin{aligned}2T=&\boldsymbol{\omega}^T[\mathbb{I}+\mu_{AB}\mathbb{X}_R\mathbb{X}_R^T+\mu_{CO}\mathbb{X}_r\mathbb{X}_r^T]\boldsymbol{\omega}\\&+\mu_{AB}[\dot{\boldsymbol{R}}^T\mathbb{X}_R^T\boldsymbol{\omega}+\boldsymbol{\omega}^T\mathbb{X}_R\dot{\boldsymbol{R}}]+\mu_{CO}[\dot{\boldsymbol{r}}^T\mathbb{X}_r^T\boldsymbol{\omega}+\boldsymbol{\omega}^T\mathbb{X}_r\dot{\boldsymbol{r}}]\\&+\mu_{AB}|\dot{\boldsymbol{R}}|^2+\mu_{CO}|\dot{\boldsymbol{r}}|^2.\end{aligned} \tag{7}$$

If we compare this general expression with the form (5) we must remember that $\boldsymbol{\omega}$ itself is not a time derivative of a certain coordinate, but is linearly related to the time derivatives of the Euler angles that relate the rotating frame $\{\vec{f}_\alpha\}$ to a space-fixed frame

$$\boldsymbol{\omega}=\mathbb{N}\begin{pmatrix}\dot{\alpha}\\\dot{\beta}\\\dot{\gamma}\end{pmatrix}. \tag{8}$$

The derivation of $\mathbb{N}$ is given in textbooks, see e.g., Ref. 20, Sec. 4–9. For future reference we give the inverse of $\mathbb{N}$ in Messiah's[21] convention of Euler angles,

$$\mathbb{N}^{-1}=\frac{1}{\sin\beta}\begin{pmatrix}-\cos\gamma&\sin\gamma&0\\\sin\beta\sin\gamma&\sin\beta\cos\gamma&0\\\cos\beta\cos\gamma&-\cos\beta\sin\gamma&\sin\beta\end{pmatrix}. \tag{9}$$

From Eqs. (7) and (8) we obtain the following expression for $2T$, while writing $\zeta=(\alpha,\beta,\gamma)$,

$$\begin{aligned}2T=&(\dot{\zeta}^T,\dot{\boldsymbol{R}}^T,\dot{\boldsymbol{r}}^T)\begin{pmatrix}\mathbb{N}^T&\mathbb{O}&\mathbb{O}\\\mathbb{O}&\mathbb{E}&\mathbb{O}\\\mathbb{O}&\mathbb{O}&\mathbb{E}\end{pmatrix}\\&\times\begin{pmatrix}\mathbb{I}+\mu_{AB}\mathbb{X}_R\mathbb{X}_R^T+\mu_{CO}\mathbb{X}_r\mathbb{X}_r^T&\mu_{AB}\mathbb{X}_R&\mu_{CO}\mathbb{X}_r\\\mu_{AB}\mathbb{X}_R^T&\mu_{AB}\mathbb{E}&\mathbb{O}\\\mu_{CO}\mathbb{X}_r^T&\mathbb{O}&\mu_{CO}\mathbb{E}\end{pmatrix}\\&\times\begin{pmatrix}\mathbb{N}&\mathbb{O}&\mathbb{O}\\\mathbb{O}&\mathbb{E}&\mathbb{O}\\\mathbb{O}&\mathbb{O}&\mathbb{E}\end{pmatrix}\begin{pmatrix}\dot{\zeta}\\\dot{\boldsymbol{R}}\\\dot{\boldsymbol{r}}\end{pmatrix}.\end{aligned} \tag{10}$$

Next we write $2T$ in terms of coordinates and conjugate momenta. A component p_μ of the linear momentum is defined by

$$p_\mu=\sum_\nu (g^{-1})_{\mu\nu}q_\nu. \tag{11}$$

This implies that we must invert the metric tensor implicitly given by Eq. (10). In order to invert the middle matrix in this expression, we may profitably use the Frobenius formula for blocked matrices[22] and obtain the classical Hamilton function

$$2T=(\boldsymbol{p}_\zeta^T,\boldsymbol{p}_R^T,\boldsymbol{p}_r^T)\begin{pmatrix} \mathbb{N}^{-1}\mathbb{I}^{-1}(\mathbb{N}^{-1})^T & -\mathbb{N}^{-1}\mathbb{I}^{-1}\mathbb{X}_R & -\mathbb{N}^{-1}\mathbb{I}^{-1}\mathbb{X}_r \\ -\mathbb{X}_R^T\mathbb{I}^{-1}(\mathbb{N}^{-1})^T & \mathbb{X}_R^T\mathbb{I}^{-1}\mathbb{X}_R+\mu_{AB}^{-1}\mathbb{E} & -\mathbb{X}_R^T\mathbb{I}^{-1}\mathbb{X}_r \\ -\mathbb{X}_r^T\mathbb{I}^{-1}(\mathbb{N}^{-1})^T & -\mathbb{X}_r^T\mathbb{I}^{-1}\mathbb{X}_R & \mathbb{X}_r^T\mathbb{I}^{-1}\mathbb{X}_r+\mu_{\mathrm{CO}}^{-1}\mathbb{E} \end{pmatrix}\begin{pmatrix} \boldsymbol{p}_\zeta \\ \boldsymbol{p}_R \\ \boldsymbol{p}_r \end{pmatrix}. \tag{12}$$

From Eq. (6) follow the angular momentum expressions

$$\mathbb{X}_R\boldsymbol{p}_R=\boldsymbol{R}\times\boldsymbol{p}_R\equiv\boldsymbol{L}, \quad \mathbb{X}_r\boldsymbol{p}_r=\boldsymbol{r}\times\boldsymbol{p}_r\equiv\boldsymbol{j}. \tag{13}$$

Further we define the total angular momentum

$$\boldsymbol{J}\equiv(\mathbb{N}^{-1})^T\boldsymbol{p}_\zeta \tag{14}$$

and write $\boldsymbol{\lambda}\equiv\boldsymbol{L}+\boldsymbol{j}$. With these definitions Eq. (12) can be written as

$$2T=(\boldsymbol{J}-\boldsymbol{\lambda})^T(\mathbb{I})^{-1}(\boldsymbol{J}-\boldsymbol{\lambda})+\frac{|\boldsymbol{p}_R|^2}{\mu_{AB}}+\frac{|\boldsymbol{p}_r|^2}{\mu_{\mathrm{CO}}}. \tag{15}$$

In order to make the transition to quantum mechanics we must replace the components of the linear momenta by the corresponding differential operators (times $-i\hbar$). However, we must be careful, since the classical Hamilton function is obviously invariant under a multiplication by the product of a scalar function and its inverse. If this function does not commute with the differential operators, the quantum mechanical expression is *not* invariant under this multiplication. Podolsky,[23] following the early work of Beltrami, pointed out that, indeed, a scalar function and its inverse must be introduced. This function is $\sqrt{g}$, where g is the determinant of the metric tensor $\{g_{\mu\nu}\}$. Again using the block structure of this tensor, we can easily derive that $g=(\mu_{AB}\mu_{\mathrm{CO}})^3\sin^2\beta\det\mathbb{I}$. By virtue of the fact that

$$\sum_i\left[\frac{\partial}{\partial\zeta_i},\sin\beta(\mathbb{N}^{-1})_{ij}\right]=0, \quad \text{for } j=1,2,3, \tag{16}$$

the square roots of the determinant of $g_{\mu\nu}$ appearing in the Podolsky formula cancel and the kinetic energy of the rotor-diatom system has exactly the classical form of Eq. (15). From Eqs. (14) and (9) we see that the vector $\boldsymbol{J}$ becomes the well-known rigid rotor angular momentum operator, with components referring to the rotating frame. The operators $\boldsymbol{L}$ and $\boldsymbol{j}$ are the usual angular momenta, as can be gathered from their definition (13). Finally,

$$\frac{|\boldsymbol{p}_R|^2}{\mu_{AB}}+\frac{|\boldsymbol{p}_r|^2}{\mu_{\mathrm{CO}}}\rightarrow-\hbar^2\left(\frac{\nabla_R^2}{\mu_{AB}}+\frac{\nabla_r^2}{\mu_{\mathrm{CO}}}\right). \tag{17}$$

If we consider the case of solid C_{60} we obtain as an additional constraint that the Euler angles $\boldsymbol{\zeta}=(\alpha,\beta,\gamma)$ are fixed. In accordance to what is stated above, we then return to classical kinematics and consider a system with only $\boldsymbol{R}$ and $\boldsymbol{r}$ as degrees of freedom. We must omit the rows and columns of the metric tensor in Eq. (10) that belong to $\boldsymbol{\zeta}$. The tensor becomes diagonal with reduced masses on the diagonal. The reduced mass μ_{AB} becomes equal to m_B, which formally follows by taking the limit $m_A\rightarrow\infty$, and the kinetic energy is that of a free CO molecule

$$2T=-\hbar^2\left(\frac{\nabla_R^2}{m_B}+\frac{\nabla_r^2}{\mu_{\mathrm{CO}}}\right), \tag{18}$$

which is not surprising since $\{\vec{f}_\alpha\}$ is now an inertial frame. This means that no terms associated with "pseudo" forces appear. Observe that we do *not* obtain the correct kinetic energy if we simply drop the terms in the Hamiltonian (15) that contain the Euler angles.

The actual computations were performed in bases of coupled spherical harmonics containing the spherical polar angles of $\boldsymbol{R}$ and $\boldsymbol{r}$, designated by Θ,Φ and θ,ϕ, respectively. The expressions of the orbital angular momenta $\boldsymbol{L}$ and $\boldsymbol{j}$, as well as of ∇_R^2 and ∇_r^2, in terms of spherical polars can be found in any textbook on quantum mechanics. We could, of course, have worked with spherical polar coordinates from the outset. The above derivations then remain essentially the same, the only difference being that the metric tensor must be transformed by a block diagonal matrix with the unit matrix and the Jacobi matrices $\mathbb{J}_R$ and $\mathbb{J}_r$ for the transformation of $\boldsymbol{R}$ and $\boldsymbol{r}$ to spherical polars on the diagonal. Since these Jacobi matrices are non-singular (except for the non-essential singular points) the inversion of the metric tensor is still easily performed.

Thus, the inversion of $g_{\mu\nu}$ is straightforward as long as we do not freeze any of the polar coordinates. However, as stated earlier, we kept the CO bond length r fixed. In that case the corresponding Jacobi matrix is of dimension 3×2 and singular. In general we should in such a case transform $g_{\mu\nu}$ explicitly with the Jacobi matrix before inversion, which is a tedious job. In the case of fixed r this procedure can be avoided, though, because a radial coordinate is orthogonal to all other coordinates in the problem. This orthogonality is easily seen if we recall that the first column of the 3×3 matrix $\mathbb{J}_r$ is the unit vector along $\boldsymbol{r}$. In view of Eq. (6) the first column of $\mathbb{X}_r\mathbb{J}_r$ vanishes. Since furthermore $\mathbb{J}_r^T\mathbb{J}_r$ is diagonal, the orthogonality follows immediately. The orthogonality has the consequence that upon freezing of r the $\partial^2/\partial r^2$ term appearing in ∇_r^2 may simply be dropped from the kinetic energy expression, without requiring any elaborate algebra.

B. Potential energy and Hamiltonian matrix elements

We modeled the intermolecular potential as a sum of atom–atom potentials

$$V(R,\Theta,\Phi,\theta,\phi)=\sum_{i\in A}\sum_{j\in B}[a_{ij}\exp(-b_{ij}r_{ij})-c_{ij}r_{ij}^{-6}]. \tag{19}$$

TABLE I. Potential parameters.

Interaction	a_{ij} (cm^{-1})	b_{ij} ($Å^{-1}$)	c_{ij} ($cm^{-1}Å^{6}$)
C–C	2.504×10^{7}	3.68	1.472×10^{5}
C–O	2.648×10^{7}	3.91	1.187×10^{5}

The dependence of the potential on the position and orientation of CO ($=B$) is through the interatomic distances r_{ij}. The parameters of the atom–atom potentials, taken from Ref. 24 are reproduced in Table I. Given its I_h symmetry, the geometry of C_{60} is solely determined by two distances: the C–C bond length in a five-ring and the interpentagon bond length. We followed Ref. 25 and took 1.455 Å and 1.398 Å, respectively, for these distances. The CO interatomic distance of 1.131 Å was calculated from B_{CO}, the ground state rotational constant of CO.[26] See Figs. 1 and 2 for two different cuts through the potential surface.

The potential has a minimum at $R_{eq}=0.192$ Å, $\Theta_{eq}=54.74°$, $\Phi_{eq}=45.00°$, $\theta_{eq}=125.26°$, $\phi_{eq}=225.00°$ with a depth of $-1073.14\ cm^{-1}$. Note that this is just one of the 20 symmetry related minima of $CO@C_{60}$. Since θ_{eq} equals exactly $\pi-\Theta_{eq}$ and $\phi_{eq}=\pi+\Phi_{eq}$, we see that $\boldsymbol{r}$ and $\boldsymbol{R}$ are anti-parallel. This is true, of course, for all 20 minima. In the minimum just mentioned the center of mass of CO is shifted into the direction of the midpoint of a six-ring at the [111] position.

The position of the minimum can be rationalized by a simple (and somewhat crude) hard sphere model. We define the "van der Waals length" l_{CO} of CO as $l_{CO}=d_{CO}+r_C+r_O$, where d_{CO} is the bond length of CO and

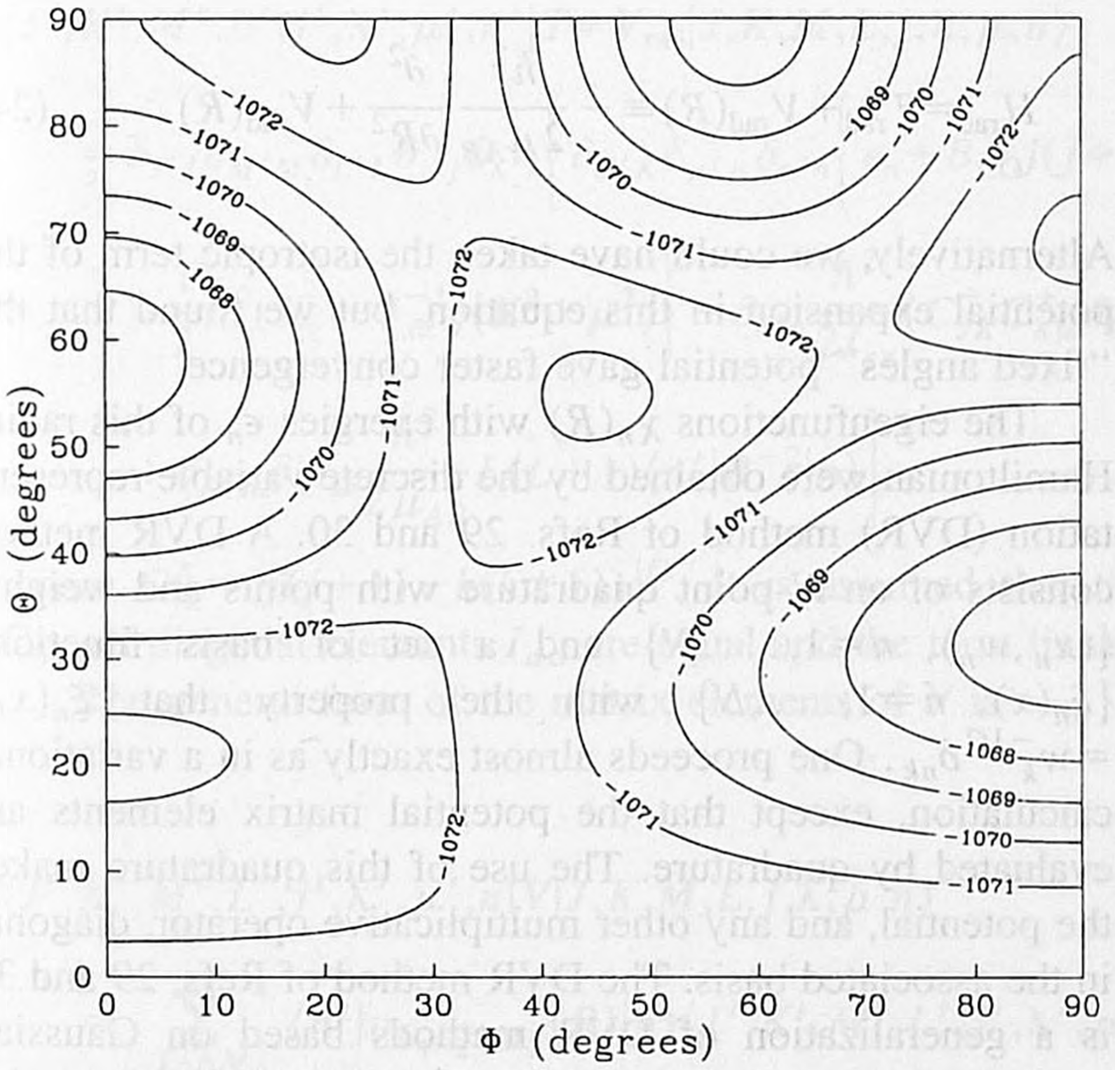

FIG. 1. Intermolecular potential (in cm^{-1}) as function of Θ and Φ with $\theta=180°-\Theta$ and $\phi=180°+\Phi$, so that CO points always in the negative radial direction. R is fixed at the equilibrium value of 0.192 Å.

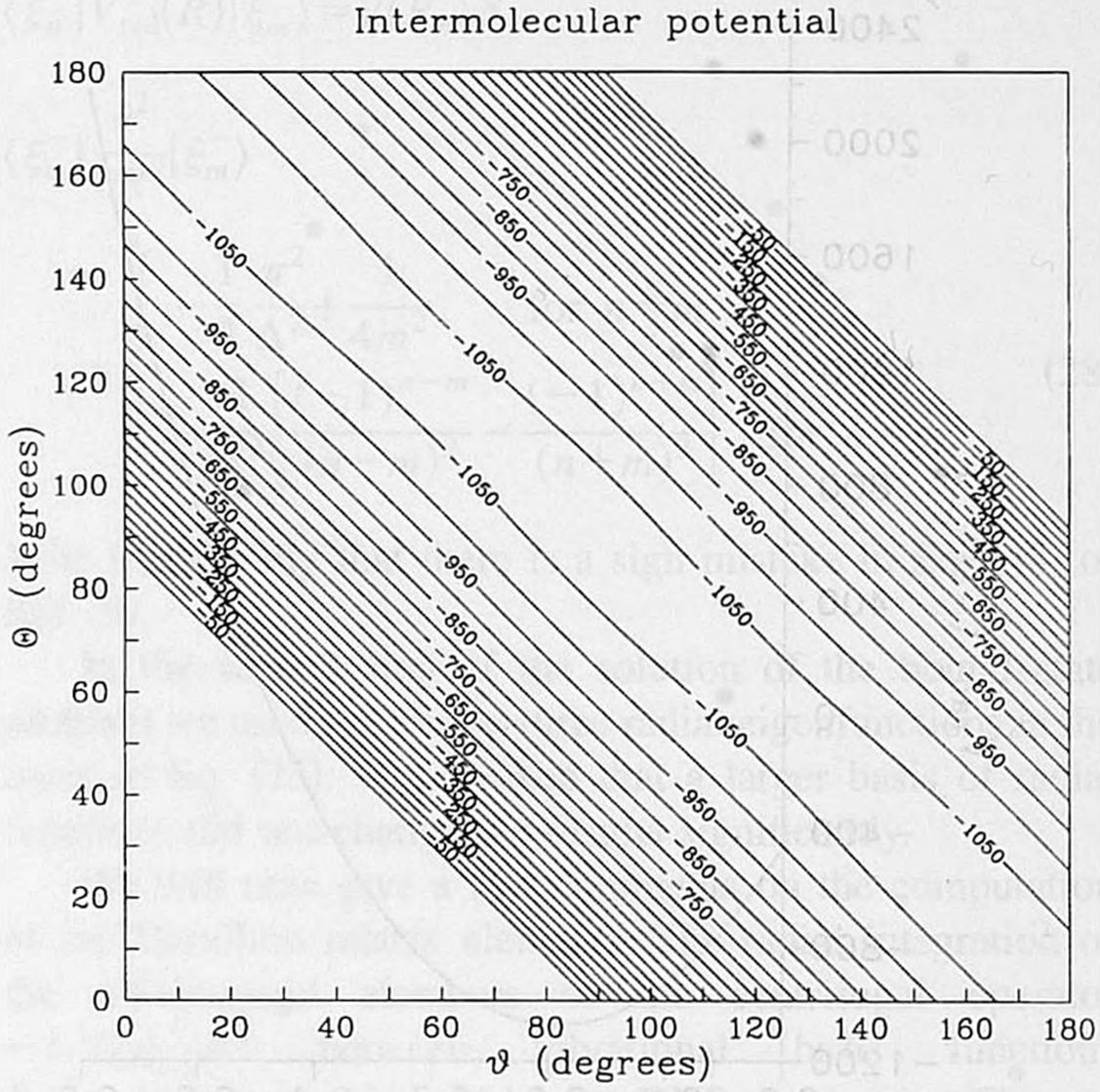

FIG. 2. Intermolecular potential (in cm^{-1}) as function of Θ and θ with $\Phi=45°$, $\phi=225°$ and $R=0.192$ Å fixed at their equilibrium values.

r_C and r_O are the van der Waals radii of carbon and oxygen, respectively. We took the respective values 1.131, 1.80, and 1.52 Å.[27] The geometric center is the center of a sphere enclosing the CO molecule with diameter l_{CO}. This center does not coincide with the nuclear mass center of CO, but is shifted by 0.22 Å towards the carbon atom. According to the model, the steric hindrance is minimal if the geometric center of CO coincides with the midpoint of C_{60}. Indeed, $R_{eq}=0.192$ Å is not far from the point of minimum repulsion. An *ab initio* calculation of the steric repulsion of CO in C_{60} by the Hartree–Fock method[12] yields $R_{eq}=0.175$ Å. We will see below that the infrared spectrum of CO can be reasonably well understood if we assume that the molecule rotates around the geometric center, rather than around its mass center. A similar model with a similar shift into the [111] direction was found to work well in solid CO.[28]

The depth of the minimum depends very strongly on the C–C bond lengths of the C_{60}. For instance, with 1.450 Å and 1.370 Å for the C–C bond lengths, which are also reasonable values, cf. Ref. 12, we found the minimum to be $-571.92\ cm^{-1}$. The position of the minimum, however, hardly changes with this change of C–C bond lengths; the equilibrium angles remain exactly the same and the equilibrium distance becomes 0.190 Å. This is not surprising since the equilibrium angles are mainly determined by the symmetry of the fullerene and the equilibrium distance R_{eq} is related to the head–tail asymmetry of the CO molecule.

Fixing the angles at their equilibrium values, we obtain from Eq. (19) a radial potential $V_{rad}(R)$. This radial potential is nearly harmonic around R_{eq}, cf. Fig. 3, with a force constant of $k=3.4\times10^{4}\ cm^{-1}Å^{-2}$. Moving (with constant $R=R_{eq}$) from one minimum to a neighboring equivalent

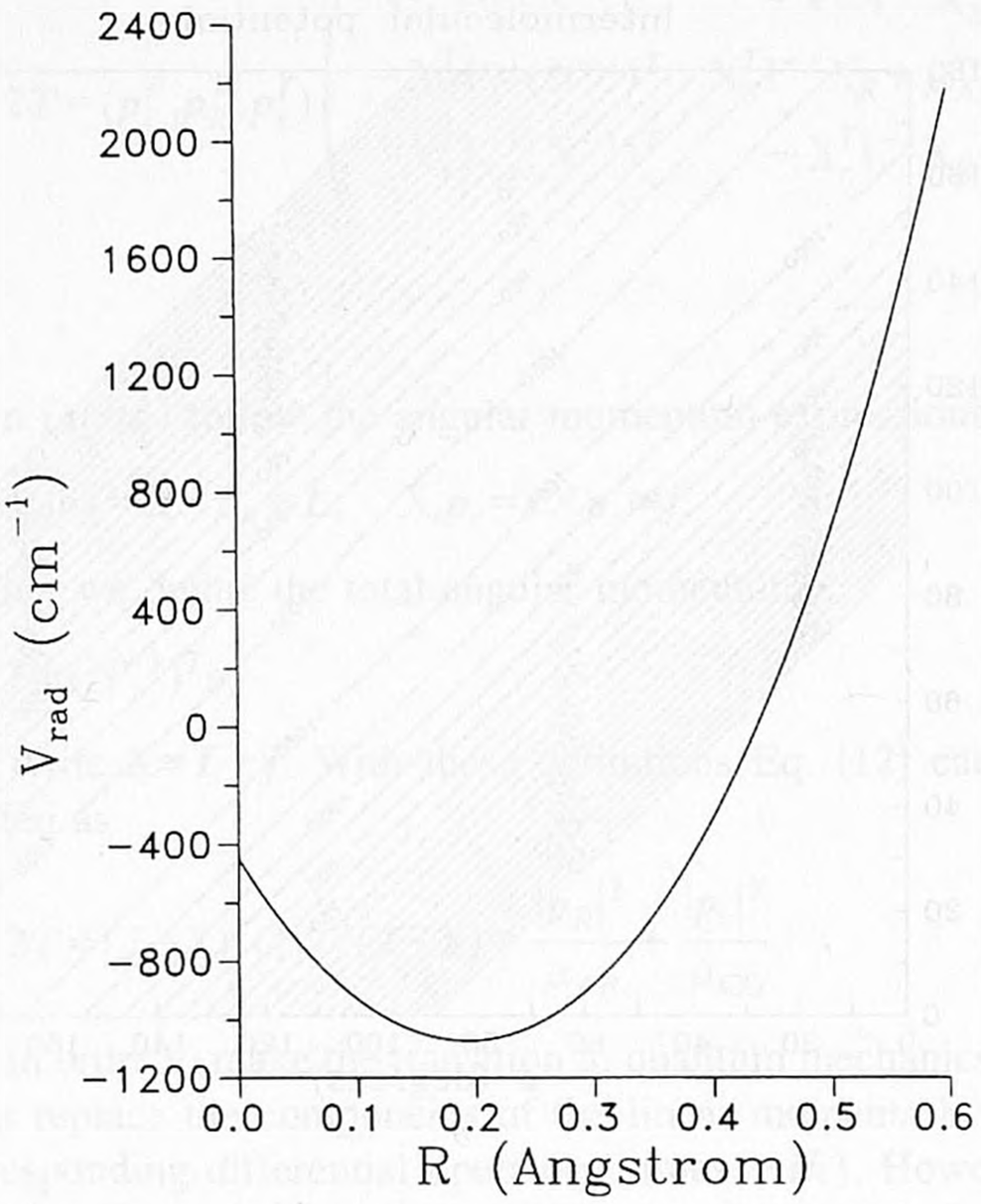

FIG. 3. Radial potential (in cm^{-1}) obtained by fixing all internal angles at their equilibrium values.

minimum, a barrier of only 1.2 cm^{-1} has to be surmounted, which shows that the potential is rather flat for motions in which $\boldsymbol{r}$ and $\boldsymbol{R}$ remain anti-parallel, see Fig. 1. If one moves away from this antiparallel orientation the potential rises steeply, see Fig. 2.

The bound states are calculated according to the Rayleigh–Ritz linear variation procedure. Before we use the potential given by Eq. (19) in this procedure, however, we expand it in terms of coupled spherical harmonics. This has the advantage that all angular matrix elements can be calculated analytically, provided that the wave function is also expanded in terms of such functions. The potential energy expansion functions $A_{L_1L_2\Lambda M_\Lambda}$ are defined by

$$A_{L_1L_2\Lambda M_\Lambda}(\Theta,\Phi,\theta,\phi)=\sum_{M_1M_2}\begin{pmatrix} L_1 & L_2 & \Lambda \\ M_1 & M_2 & M_\Lambda \end{pmatrix} \times C^{(L_1)}_{M_1}(\Theta,\Phi)C^{(L_2)}_{M_2}(\theta,\phi), \quad (20)$$

where the $C^{(L)}_M$ are spherical harmonics in Racah normalization. The quantity in parentheses is a Wigner $3j$-symbol. Note that the functions $A_{L_1L_2\Lambda M_\Lambda}$ are not normalized to unity, they are orthogonal, however. The potential, Eq. (19), can be written as follows:

$$V(R,\Theta,\Phi,\theta,\phi)=\sum_{L_1L_2\Lambda M_\Lambda} v_{L_1L_2\Lambda M_\Lambda}(R) \times A_{L_1L_2\Lambda M_\Lambda}(\Theta,\Phi,\theta,\phi). \quad (21)$$

The Fourier coefficients $v_{L_1L_2\Lambda M_\Lambda}(R)$ are defined by

$$v_{L_1L_2\Lambda M_\Lambda}(R)=\frac{(2L_1+1)(2L_2+1)(2\Lambda+1)}{16\pi^2} \times\int_0^\pi\int_0^{2\pi}\int_0^\pi\int_0^{2\pi} A^*_{L_1L_2\Lambda M_\Lambda}(\Theta,\Phi,\theta,\phi) \times V(R,\Theta,\Phi,\theta,\phi)\sin\Theta\sin\theta\, d\Theta d\Phi d\theta d\phi. \quad (22)$$

In practice this integration is performed numerically, with 15-point Gauss–Legendre grids for the integration over Θ and θ, and 15-point Gauss–Chebyshev grids for the integration over Φ and ϕ. This implies that the expansion in Eq. (21) must be truncated.

A convenient basis for the calculation of Hamiltonian matrix elements is the following

$$|J,K,M,L,j,\lambda,\mu,n\rangle =[(2J+1)/8\pi^2]^{1/2}D^{(J)}_{MK}(\alpha,\beta,\gamma)^*R^{-1}\chi_n(R) \times\sum_{m_Lm_j}\langle Lm_L;jm_j|\lambda\mu\rangle Y^{(L)}_{m_L}(\Theta,\Phi)Y^{(j)}_{m_j}(\theta,\phi). \quad (23)$$

The quantity in pointed brackets is a Clebsch–Gordan coefficient and the functions $R^{-1}\chi_n$ are radial basis functions to which we will return shortly. The functions $Y^{(\lambda)}_\mu$ are normalized spherical harmonics. These functions are multiplied by the Wigner functions $D^{(J)}_{MK}(\alpha,\beta,\gamma)^*$, which contain the Euler angles of the rotating frame $\{\vec{f}_\alpha\}$.

The bound state problem was solved in two steps. In the first step we determined the radial basis functions. To that end we considered the "fixed angles" radial potential $V_{rad}(R)$ introduced above, and diagonalized the Hamiltonian

$$H_{rad}=T_{rad}+V_{rad}(R)\equiv-\frac{\hbar^2}{2\mu_{AB}}\frac{\partial^2}{\partial R^2}+V_{rad}(R). \quad (24)$$

Alternatively, we could have taken the isotropic term of the potential expansion in this equation, but we found that the "fixed angles" potential gave faster convergence.

The eigenfunctions $\chi_n(R)$ with energies ϵ_n of this radial Hamiltonian were obtained by the discrete variable representation (DVR) method of Refs. 29 and 30. A DVR method consists of an N-point quadrature with points and weights $\{(x_n,w_n),\ n=1,\ldots,N\}$ and a set of basis functions $\{\xi_n(x),\ n=1,\ldots,N\}$ with the property that $\xi_n(x_k)=w_k^{-1/2}\delta_{nk}$. One proceeds almost exactly as in a variational calculation, except that the potential matrix elements are evaluated by quadrature. The use of this quadrature makes the potential, and any other multiplicative operator, diagonal in the associated basis. The DVR method of Refs. 29 and 30 is a generalization of DVR methods based on Gaussian quadratures, with their associated bases of orthogonal polynomials.

For the range $x=(-\infty,\infty)$, appropriate basis functions satisfying the DVR conditions are

$$\xi_n(x)=\Delta^{-1/2}\,\mathrm{sinc}\left[\pi\left(\frac{x}{\Delta}-n\right)\right]\equiv\Delta^{-1/2}\frac{\sin\,\pi(x/\Delta-n)}{\pi(x/\Delta-n)}. \tag{25}$$

The corresponding quadrature is $\{(x_n,w_n)=(n\Delta,\Delta),\ n=-N,\ldots,N\}$, in which the parameter Δ is the grid spacing. The wave function outside the grid is effectively zero, which is equivalent to the assumption that the potential in this region is infinitely high. By choosing the border of the grid at a high value of the potential, the accuracy of the lowest states can become very high. Since the range for R is $[0,\infty)$, we obtained the wave functions $\chi_n(R)$ using the following DVR:

$$\{(R_n,w_n)=(n\Delta,\Delta),\ \ n=1,\ldots,N\} \tag{26}$$

with the basis functions

$$\xi_n^-(R)=\xi_n(R)-\xi_n(-R), \tag{27}$$

the so-called[30] "wrapped" sinc functions. Since $R^{-1}\chi_n(R)$ must be finite at $R=0$, cf. Eq. (23), $\chi_n(R)$ has to vanish at $R=0$ and thus the basis functions $\xi_n^-(R)$ have the correct behavior at $R=0$. The matrix elements of the operators $V_{\mathrm{rad}}(R)$ and $\partial^2/\partial R^2$ are derived in Refs. 29 and 30

$$\langle\xi_n^-|V_{\mathrm{rad}}(R)|\xi_m^-\rangle=V(R_n)\,\delta_{nm}$$

$$\langle\xi_n^-|\frac{\partial^2}{\partial R^2}|\xi_m^-\rangle$$

$$=\begin{cases}-\frac{1}{3}\frac{\pi^2}{\Delta^2}+\frac{1}{4m^2} & \text{for } n=m\\ -\frac{2}{\Delta^2}\left[\frac{(-1)^{n-m}}{(n-m)^2}-\frac{(-1)^{n+m}}{(n+m)^2}\right] & \text{for } n\neq m.\end{cases} \tag{28}$$

Note incidentally that there is a sign mistake in Eq. (48) of Ref. 30.

In the second step of the solution of the bound state problem we used the lowest three radial eigenfunctions in the basis of Eq. (23). We checked that a larger basis of radial functions did not change the results significantly.

We will now give a few comments on the computation of the Hamilton matrix elements. The radial integration of the off-diagonal elements of the centrifugal operator $-L^2/2\mu_{AB}R^2$ between vibrational basis functions $R^{-1}\chi_n(R)$ was performed by the DVR quadrature. The operator L^2 is diagonal in the angular basis. The DVR quadrature of Eq. (26) was also used for the radial potential terms $\langle n'|v_{L_1L_2\Lambda M_\Lambda}(R)|n\rangle$. These elements are calculated in advance and stored.

The cross term $\boldsymbol{J}^T(\mathbb{I})^{-1}\boldsymbol{\lambda}$ couples functions with different K and μ in bra and ket. For the $J=0$ state, however, the matrix elements due to these cross terms vanish. The radial kinetic energy operator is not diagonal in the basis of Eq. (23), but the sum $T_{\mathrm{rad}}+V_{\mathrm{rad}}$ is. Therefore, it is convenient to consider $T+V_{\mathrm{rad}}$, and to subtract later the matrix elements of V_{rad}. We find the general matrix element

$$\begin{aligned}&\langle J',K',M',L',j',\lambda',\mu',n'|T+V_{\mathrm{rad}}|J,K,M,L,j,\lambda,\mu,n\rangle\\ &=\delta_{J'J}\delta_{M'M}\delta_{L'L}\delta_{j'j}\delta_{\lambda'\lambda}\Bigg[\delta_{K'K}\delta_{\mu'\mu}\delta_{n'n}\Bigg\{\epsilon_n+B_{\mathrm{CO}}j(j+1)+\frac{\hbar^2}{2I_{xx}}(J(J+1)+\lambda(\lambda+1))-\frac{\hbar^2}{I_{zz}}K\mu\\ &\quad+\frac{1}{2}\hbar^2(I_{zz}^{-1}-I_{xx}^{-1})(K^2+\mu^2)\Bigg\}-\delta_{n'n}\frac{\hbar^2}{2I_{xx}}(C_{JK}^{+}C_{\lambda\mu}^{+}\delta_{K'K+1}\delta_{\mu'\mu+1}+C_{JK}^{-}C_{\lambda\mu}^{-}\delta_{K'K-1}\delta_{\mu'\mu-1})\\ &\quad+\delta_{K'K}\delta_{\mu'\mu}\frac{\hbar^2}{2\mu_{AB}}L(L+1)\langle n'|R^{-2}|n\rangle\Bigg],\end{aligned} \tag{29}$$

where $C_{jk}^{\pm}=(j(j+1)-k(k\pm1))^{1/2}$. It is assumed that the rotor is a symmetric top, i.e., that $I_{xx}=I_{yy}$. In the case of C_{60} all diagonal elements $I_{\alpha\alpha}$ are equal and the term linear in $K^2+\mu^2$ vanishes.

The general form of the matrix elements of V is

$$\begin{aligned}&\langle J',K',M',L',j',\lambda',\mu',n|V|J,K,M,L,j,\lambda,\mu,n\rangle\\ &=\sum_{L_1L_2\Lambda M_\Lambda}\langle n'|v_{L_1L_2\Lambda M_\Lambda}(R)|n\rangle\langle J',K',M',L',j',\lambda',\mu'|A_{L_1L_2\Lambda M_\Lambda}|J,K,M,L,j,\lambda,\mu\rangle,\end{aligned} \tag{30}$$

where the angular matrix elements are

$$\langle J',K',M',L',j',\lambda',\mu'|A_{L_1L_2\Lambda M_\Lambda}|J,K,M,L,j,\lambda,\mu\rangle$$
$$=(-1)^{L+j+\mu+\lambda'}\delta_{J'J}\delta_{K'K}\delta_{M'M}[(2\lambda'+1)(2\lambda+1)(2L'+1)(2L+1)(2j'+1)(2j+1)]^{1/2}$$
$$\times\begin{pmatrix}L' & L_1 & L\\ 0 & 0 & 0\end{pmatrix}\begin{pmatrix}j' & L_2 & j\\ 0 & 0 & 0\end{pmatrix}\begin{pmatrix}\lambda' & \Lambda & \lambda\\ \mu' & M_\Lambda & -\mu\end{pmatrix}\begin{Bmatrix}L' & L_1 & L\\ j' & L_2 & j\\ \lambda' & \Lambda & \lambda\end{Bmatrix}. \tag{31}$$

The quantity in curly brackets is a $9j$-symbol. The operator $V_{\rm rad}$, which is diagonal in the radial basis, must be subtracted from V since it is already included in ϵ_n. It will only contribute to the matrix elements $\langle n'|v_{0000}(R)-V_{\rm rad}|n\rangle$.

In calculations on non-rotating C_{60}, Eq. (18), we have to use a basis that is similar to that of Eq. (23), except that it lacks the Wigner D functions. This basis has only five quantum numbers: L, j, λ, μ, and n. The matrix elements of the potential energy operator in this basis are equal to the matrix elements of Eq. (31), except for the missing Kronecker deltas for J, K, and M. The matrix elements of the kinetic energy operator of Eq. (18) plus radial potential in the five dimensional basis are

$$\langle L',j',\lambda',\mu',n'|T+V_{\rm rad}|L,j,\lambda,\mu,n\rangle$$
$$=\delta_{L'L}\delta_{j'j}\delta_{\lambda'\lambda}\delta_{\mu'\mu}\Big[\delta_{n'n}(\epsilon_n+B_{\rm CO}j(j+1))$$
$$+\frac{\hbar^2}{2m_B}L(L+1)\langle n'|R^{-2}|n\rangle\Big]. \tag{32}$$

C. Infrared intensities

As stated in the introduction, experiments are planned to measure the spectrum of $CO@C_{60}$ in the infrared or far-infrared region. We will now briefly discuss the *ab initio* calculation of this spectrum. For the far-infrared transitions that correspond to the vibrations and (hindered) rotations of (rigid) CO in C_{60} the dipole operator is approximated simply by the permanent dipole $\mu^{\rm CO}$ of the CO molecule. Thus we neglect all the terms due to the interaction of the bucky ball and the diatom. The dipole operator expressed with respect to the frame fixed on C_{60} is

$$\mu_\nu^{\rm BF}=\mu^{\rm CO}C_\nu^{(1)}(\theta,\phi). \tag{33}$$

If we want to study the van der Waals side bands of the fundamental stretch of CO in the infrared region, then (neglecting the coupling of the intramonomer and intermonomer vibrations) we have to use the monomer vibrational transition dipole

$$\mu^{01}=\langle 0|\mu(r)|1\rangle \tag{34}$$

instead of the permanent dipole. However, since the two dipoles have the same angular dependence, the theory for the line intensities of the far- and mid-infrared part of the spectrum is the same.

In the case of fixed C_{60} the line strength of the transition from E_i to E_f, where $\psi_{i,\tau}$ and $\psi_{f,\tau'}$ are the (degenerate) wave functions belonging to these energies, is defined as

$$S(f\leftarrow i)=\sum_\nu\sum_{\tau\tau'}|\langle\psi_{f,\tau'}|\mu_\nu|\psi_{i,\tau}\rangle|^2. \tag{35}$$

This leads to a temperature dependent absorption coefficient $I(f\leftarrow i)$ that is given by

$$I(f\leftarrow i)=Z^{-1}(E_f-E_i)[\exp(-E_i/kT)-\exp(-E_f/kT)]S(f\leftarrow i), \tag{36}$$

where Z is the partition function $Z=\Sigma_i n_i\exp(-E_i/kT)$ and n_i is the degeneracy of level E_i. In the actual calculations we did not evaluate Z, because we only look at relative intensities at the same temperature (77 K). The line strength in Eq. (35) will be expressed in units of μ_T^2, where μ_T is either μ^{01} or $\mu^{\rm CO}$. The shielding of the CO (transition) dipole by C_{60} may lead to a reduction of the line strengths, but will not change the relative intensities.

For freely rotating $CO@C_{60}$ different formulas have to be used, because in that case we have three extra degrees of freedom and J and M are good quantum numbers. The dipole operator expressed relative to the space fixed frame is

$$\mu_m^{\rm SF}=\sum_\nu D_{m\nu}^{(1)}(\alpha,\beta,\gamma)^*\mu_\nu^{\rm BF}. \tag{37}$$

The formula for the line strength of a transition from (i,J) to (f,J') is now[31]

$$S(f,J'\leftarrow i,J)=\sum_{M'mM}|\langle\psi_f^{J'M'}|\mu_m^{\rm SF}|\psi_i^{JM}\rangle|^2. \tag{38}$$

The quantity in Eq. (38) can now be substituted into the equivalent of Eq. (36), yielding

$$I(f,J'\leftarrow i,J)=g_iZ^{-1}(E_{f,J'}-E_{i,J})[\exp(-E_{i,J}/kT)-\exp(-E_{f,J'}/kT)]S(f,J'\leftarrow i,J), \tag{39}$$

where g_i is the nuclear spin statistical weight of the state (i,J) [and of the final state (f,J')] and the partition function is now defined as $Z=\Sigma_{i,J}g_i(2J+1)\exp(-E_{i,J}/kT)$.

III. SYMMETRY

When considering the symmetry of the complex $CO@C_{60}$, we have to distinguish its free and solid form. In the case of solid, nonrotating, C_{60}, the icosahedral buckyball cage provides to CO an external potential with symmetry group I_h. In the case of a complex rotating in free space, we have to consider the permutation inversion (PI) group[32] instead of the point group I_h. The PI group consists of the permutations of the carbon atoms that lead to observable splittings, the so-called feasible permutations. Further it contains the space-inversion (parity) operator E^*. If C_{60} is rigid, the PI group of $CO@C_{60}$ is isomorphic with the point group I_h and will be referred to as $PI(I_h)$. This group is a direct product: $PI(I_h) = PI(I)\otimes\{E,E^*\}$, where E is the identity operator. The group $PI(I_h)$ is generated by four generators: three permutations that we denote by $\pi(C_{2y})$, $\pi(C_3)$ and $\pi(C_5)$, and E^*. The permutation $\pi(C_{2y})$ is equivalent to a rotation of C_{60} around its y axis over 180°. The second permutation $\pi(C_3)$ is equivalent to a rotation over 120° around an axis in the [111] direction. The third generator is the permutation $\pi(C_5)$ that is equivalent to a rotation over 72° around an axis in the xz plane which is 31.72° off the x axis.

The group I has five irreducible representations (irreps): A, T_1, T_2, G, and H of dimension one, three, three, four, and five, respectively. The ten irreps of I_h are obtained from those of I by adding the g/u parity label. The character table of I_h can be found in Ref. 33. Although bases spanning the irreps of I_h or $PI(I_h)$ reduce as much as is possible the size of the secular problems, we rather worked with bases transforming according to the irreps of the Abelian subgroups D_{2h} and $PI(D_{2h})$, respectively. The reason for this is that we did not want to restrict our computer programs to the special highly symmetric case of $CO@C_{60}$. Also the construction and programming of basis functions adapted to the full icosahedral symmetry is rather complicated, while the construction of a basis adapted to D_{2h} is straightforward. However, the analysis of the final wave functions and transition probabilities will be performed in terms of the full I_h symmetry.

We will briefly illustrate the action of the elements of I_h and $PI(I_h)$ on the coordinates and on the basis functions. The difference between these two groups is that in the second case the coordinates are defined relative to a rotating frame, which itself is affected by the elements of $PI(I_h)$. As an example we show the effect of E^* giving $\vec{f}'_x=E^*\vec{f}_x=-\vec{f}_x$ and $\vec{f}'_y=E^*\vec{f}_y=-\vec{f}_y$. The body fixed z axis is defined as $\vec{f}_z=\vec{f}_x\times\vec{f}_y$, so the new z axis is $\vec{f}'_x\times\vec{f}'_y=\vec{f}'_z=\vec{f}_z$. Because of this definition of $\vec{f}_z$, E^* maps a right-handed frame onto a right-handed frame and accordingly its action on the Euler angles is well defined. In short

TABLE II. Effect of the symmetry group generators on the basis functions.

D_{2h}		
C_{2x}	$(-1)^{\lambda}$	$\lvert L,j,\lambda,-\mu\rangle$
C_{2y}	$(-1)^{\lambda+\mu}$	$\lvert L,j,\lambda,-\mu\rangle$
i	$(-1)^{L+j}$	$\lvert L,j,\lambda,\mu\rangle$
$PI(D_{2h})$		
$\pi(C_{2x})$	$(-1)^{J+\lambda}$	$\lvert J,-K,M,L,j,\lambda,-\mu\rangle$
$\pi(C_{2y})$	$(-1)^{J+K+\lambda-\mu}$	$\lvert J,-K,M,L,j,\lambda,-\mu\rangle$
E^*	$(-1)^{K+L+j+\mu}$	$\lvert J,K,M,L,j,\lambda,\mu\rangle$

$$\{\vec{f}'_\alpha\}=E^*\{\vec{f}_\alpha\}=\{\vec{f}_\alpha\}\begin{pmatrix}-1&0&0\\0&-1&0\\0&0&1\end{pmatrix}=\{\vec{f}_\alpha\}\mathbb{R}_z(\pi). \tag{40}$$

So, E^* is equivalent to a rotation C_{2z} over π around the z axis [with matrix $\mathbb{R}_z(\pi)$]. From the definition of the Euler angles α,β,γ that relate the body-fixed frame to a space-fixed frame by the rotation $\mathbb{R}_{zyz}(\alpha,\beta,\gamma)$, it follows that the Euler angles α',β',γ' of the frame mapped by E^* must satisfy the relation

$$\mathbb{R}_z(\alpha')\mathbb{R}_y(\beta')\mathbb{R}_z(\gamma')=\mathbb{R}_z(\alpha)\mathbb{R}_y(\beta)\mathbb{R}_z(\gamma)\mathbb{R}_z(\pi), \tag{41}$$

from which immediately follows that $\alpha'=\alpha$, $\beta'=\beta$, and $\gamma'=\gamma+\pi$.

The operation E^* inverts the position vectors of the atoms of CO, which are given in terms of the vectors $\vec{R}$ and $\vec{r}$ by

$$\vec{r}_C=\vec{R}+\zeta\vec{r} \quad \text{and} \quad \vec{r}_O=\vec{R}+(\zeta-1)\vec{r}, \tag{42}$$

where the quantity ζ is the mass ratio m_O/M_{CO}. The vectors $\vec{R}$ and $\vec{r}$ are also inverted. Since the component vectors $\boldsymbol{R}$ and $\boldsymbol{r}$ are defined with respect to the body-fixed frame, it follows that

$$\boldsymbol{R}'=-\mathbb{R}_z(\pi)\boldsymbol{R} \text{ and } \boldsymbol{r}'=-\mathbb{R}_z(\pi)\boldsymbol{r}. \tag{43}$$

It is easily derived that this implies for the angular coordinates that $\Theta'=\pi-\Theta,\Phi'=\Phi$ and $\theta'=\pi-\theta,\phi'=\phi$.

The effect of E^* on the basis functions is readily found. For the external functions we may write,

$$\begin{aligned}E^*D^{(J)}_{M,K}(\alpha,\beta,\gamma)^*&=D^{(J)}_{M,K}(\alpha,\beta,\gamma+\pi)^*\\&=(-1)^KD^{(J)}_{M,K}(\alpha,\beta,\gamma)^*.\end{aligned} \tag{44}$$

From the general relation $Y^{(l)}_m(\pi-\theta,\phi)=(-1)^{l+m}\times Y^{(l)}_m(\theta,\phi)$ follows that the internal functions (for which $m_L+m_j=\mu$) transform as

$$\begin{aligned}E^*\lvert L,j,\lambda,\mu\rangle=\sum_{m_Lm_j}&Y^{(L)}_{m_L}(\pi-\Theta,\Phi)Y^{(j)}_{m_j}(\pi-\theta,\phi)\\&\times\langle Lm_L;jm_j\rvert\lambda\mu\rangle\\&=(-1)^{L+j+\mu}\lvert L,j,\lambda,\mu\rangle,\end{aligned} \tag{45}$$

so that the effect of E^* on the angular basis in Eq. (23) is as given in Table II.

TABLE III. Subduction of the $(2\lambda+1)$-dimensional irreps of $SO(3)$ carried by the spherical harmonics $Y_\mu^{(\lambda)}$ to the icosahedral group I.

λ	A	T_1	T_2	G	H
0	1	0	0	0	0
1	0	1	0	0	0
2	0	0	0	0	1
3	0	0	1	1	0
4	0	0	0	1	1
5	0	1	1	0	1
6	1	1	0	1	1
7	0	1	1	1	1
8	0	0	1	1	2
9	0	1	1	2	1
10	1	1	1	1	2
11	0	2	1	1	2
12	1	1	1	2	2
13	0	1	2	2	2
14	0	1	1	2	3
15	1	2	2	2	2

In the case that the C_{60} monomer is fixed, with symmetry group I_h, the inversion operator $i \in I_h$ inverts the position vectors of all atoms in the system. The angular basis functions, depending on the internal angles Θ,Φ and θ,ϕ, have a definite parity $L+j$ and inversion leads to a simple multiplication of each basis function by a factor $(-1)^{L+j}$.

In a similar way one derives, for instance, that the effect on the internal angles Θ,Φ and θ,ϕ of the rotation $C_{2y} \in I_h$ is the same as the effect of $\pi(C_{2y}) \in \mathrm{PI}(I_h)$. The same equivalence between rotations and permutations holds for the other generators. Since the actual calculations were performed in D_{2h}[or $\mathrm{PI}(D_{2h})$] symmetry, we just give the effect of the generators of these groups on the basis functions in Table II. These transformation rules and the character table of D_{2h} allow us to create bases adapted to D_{2h} or $\mathrm{PI}(D_{2h})$.

We shall now look in particular at the symmetric irrep A_g of I_h or $\mathrm{PI}(I_h)$, since the potential energy operator transforms according to this irrep. By taking linear combinations of the angular expansion functions $A_{L_1L_2\Lambda M_\Lambda}$ of Eq. (20) it is possible to reduce the number of expansion coefficients in the potential enormously. It can be derived that functions transforming as A_g must have $\Lambda=0,6,10,12,15,\ldots$, cf. Table III. Moreover, it can be shown that only specific linear combinations of functions $A_{L_1L_2\Lambda M_\Lambda}$, in short $A_{\Lambda M_\Lambda}$, span an A_g function. For example, all basis functions with $\Lambda=M_\Lambda=0$ transform as A_g and for $\Lambda=6$ only the combinations

$$A_{6,0}+\sqrt{\tfrac{21}{4}}(A_{6,2}+A_{6,-2})-\sqrt{\tfrac{7}{2}}(A_{6,4}+A_{6,-4}) -\sqrt{\tfrac{105}{44}}(A_{6,6}+A_{6,-6}) \quad (46)$$

with even values of L_1+L_2 transform as A_g.

The dipole operator used to calculate the transition intensities of the complex $CO@C_{60}$ with C_{60} fixed is given by Eq. (33) with $\nu=0,\pm1$. This operator is an irreducible tensor operator transforming as T_{1u} under I_h. This leads to the selection rules $A\leftrightarrow T_1$, $T_2\leftrightarrow G$, $T_2\leftrightarrow H$, $T_1\leftrightarrow H$, $G\leftrightarrow H$, $H\leftrightarrow H$, $T_1\leftrightarrow T_1$, and $G\leftrightarrow G$, in combination with an obligatory change of parity: $g\leftrightarrow u$.

For the freely rotating complex the dipole operator is given by Eq. (37). Since it must be invariant under all permutations and change sign under E^*, it follows that each component μ_m^{SF} of this dipole operator transforms as A_u of $\mathrm{PI}(I_h)$. Transitions must obey the parity selection rule: $g\leftrightarrow u$, and they must stay within the same irrep of the permutation group $\mathrm{PI}(I)$. These are the exact selection rules. In addition, there are approximate selection rules that apply to the internal part of the wave functions. These rules are given by the transformation properties of the operator μ_ν^{BF} in Eq. (33). The components with $\nu=0,\pm1$ of this operator carry the irrep T_1 of the pure permutation group $\mathrm{PI}(I)$. Also the corresponding components of the rotation function $D^{(1)}_{m\nu}(\alpha,\beta,\gamma)^*$ in Eq. (37) carry this irrep (see Table III), so that the total dipole μ_m^{SF} is indeed invariant under $\mathrm{PI}(I)$. The internal dipole components and the rotation functions in Eq. (37) with $\nu=\pm1$ do not have a definite parity with respect to E^*, however, so there are no general selection rules regarding the internal and rotational transitions that concern the parity. But, otherwise, the internal selection rules are identical to the rules that must be obeyed by the complex with fixed C_{60}. They are valid to the extent that one can separate the internal motions of the complex from its overall rotation. The coupling between these internal motions and the overall rotation is given by the cross terms $2\boldsymbol{\lambda}^T\mathbb{I}^{-1}\boldsymbol{J}$ in the kinetic energy operator of Eq. (15).

IV. NUMERICAL DETAILS AND RESULTS

Before we present the results of our calculations, we give some technical information. The potential was expanded in angular functions up to and including $L_1=8$ and $L_2=8$. We only retain the functions $A_{L_1L_2\Lambda M_\Lambda}$ with $\Lambda=0$ and $\Lambda=6$. The next set of functions of A_g symmetry has $\Lambda=10$ and we checked that this set gives a negligible contribution to the potential. In total, the expanded potential consists of 219 angular functions, which reproduces the original atom–atom potential to within about 0.1% over the whole range of R and for all angles.

The radial basis functions determined by the DVR method are described in Sec. II. We used a grid of 30 points, spaced by 0.025 Å. The potential at the outermost gridpoint at $R=0.75$ Å is 5713 cm^{-1}. The lowest three eigenvalues of the radial Hamiltonian in Eq. (24) are -971.88, -765.05, and -544.86 cm^{-1} respectively, so the radial excitation energies are 206.83 and 427.02 cm^{-1}. Since the radial zero-point energy is 101.26 cm^{-1}, we observe that the radial problem is rather harmonic. The values of the wave functions at the last gridpoint $R=0.75$ Å are 8 to 9 orders of magnitude smaller than the maximum values, which shows that the grid is sufficiently large to ensure convergence. In Ref. 29 it is recommended to use at least four grid points per De Broglie wavelength. In our case the third radial wave function still has 12 grid points per De Broglie wavelength.

TABLE IV. Energy levels (in cm^{-1}) of the complex $CO@C_{60}$ for the full potential (I_h symmetry) and for the $\Lambda=0$ potential [$O(3)$ symmetry]. The (+) or (−) refers to the parity σ of each ladder, the g/u parity of the levels is $\sigma(-1)^{\lambda}$, see text.

λ	irrep	$O(3)$	I_h	$O(3)$	I_h	$O(3)$	I_h	$O(3)$	I_h
Ladder		1(+)		2(+)		3(−)		4(+)	
0	A	−809.76	−809.81					−600.37	−600.49
1	T_1	−806.32	−806.37	−646.30	−646.34	−645.86	−645.89	−596.46	−596.33
2	H	−799.42	−799.49	−640.30	−640.32	−638.95	−639.00	−588.66	−588.75
3	G	−789.08	−789.86	−631.10	−630.90	−628.60	−628.07	−576.90	−577.77
	T_2		−788.13		−631.50		−629.44		−575.83
4	G	−775.26	−776.05	−618.30	−618.46	−614.70	−614.53	−560.65	−561.51
	H		−774.63		−618.19		−614.83		−559.97
5	T_2	−757.71	−758.35	−600.61	−601.04	−596.78	−596.89	−538.30	−538.88
	H		−757.93		−600.68		−596.80		−538.46
	T_1		−756.70		−600.17		−596.65		−537.20
6	G	−735.35	−735.97	−575.97	−576.50	−573.26	−573.43	−506.80	−507.45
	H		−735.52		−576.11		−573.33		−506.98
	T_1		−734.67		−575.41		−573.00		−506.11
	A		−733.95		−574.77		−572.80		−505.39
7	G	−705.23	−705.85	−542.16	−542.77	−540.58	−540.86	−462.47	−463.08
	T_2		−705.65		−542.68		−540.79		−462.97
	H		−705.09		−542.09		−540.52		−462.35
	T_1		−704.16		−541.11		−540.09		−461.48
8	H	−662.54	−663.21	−495.07	−495.76	−493.91	−494.27	−402.73	−403.35
	T_2		−662.80		−495.35		−494.05		−402.95
	G		−662.61		−495.13		−493.95		−402.58
	H		−661.64		−494.10		−493.42		−401.89
9	T_1	−603.16	−604.04	−426.01	−426.77	−430.07	−430.56		
	H		−603.65		−426.47		−430.36		
	G		−603.40		−426.26		−430.22		
	G		−602.38		−425.19		−429.61		
	T_2		−602.34		−425.14		−429.58		

The maximum value of the quantum number j in the angular basis is $j_{max}=9$. We take also the maximum L equal to this value, cf. Eq. (23). All possible λ values for a given combination of j and L were included in the basis. We checked that the value $j_{max}=9$ is sufficiently large to get energy levels converged to within about 0.01 cm^{-1}.

A. Energy levels

The levels from the five-dimensional calculations with C_{60} fixed are listed in Table IV. Also shown are the levels from a calculation in which only the $\Lambda=0$ terms of the potential expansion are included. In this case the potential is invariant under a simultaneous rotation of the vector $\boldsymbol{R}$, which gives the position of the CO center of mass, and the vector $\boldsymbol{r}$, which describes the CO orientation. By the ordering of the levels in Table IV we illustrate that the structure of the calculated energy level diagram can be understood in terms of three basic features. In the first place, as is most clearly observed in the levels calculated from the $\Lambda=0$ potential, there are a number of ladders which are similar to the ladder of rotational levels of free CO. If we look at the eigenvectors, however, we must conclude that the quantum number j, which describes the CO rotation, is not at all a good quantum number. Strong mixing occurs between basis functions with different j and L. The rungs of the ladders are in fact labeled by the quantum number λ, rather than by j. If the potential expansion is restricted to the $\Lambda=0$ terms λ is an exact quantum number, in the calculations with the full potential λ is nearly conserved. So the rotational ladders do not correspond to the nearly free rotation of CO, i.e., of the vector $\boldsymbol{r}$, but rather to the rotation of $\boldsymbol{r}$ and $\boldsymbol{R}$ simultaneously. We observe that the rotational spacings are significantly different from those of free CO. A rotational constant can be defined for each ladder by fitting its $\Lambda=0$ levels to the expression $B\lambda(\lambda+1)$. The values of B in Table V are obtained by doing this for the levels up to $\lambda=5$ inclusive. For the lowest ladder this yields $B=1.73$ cm^{-1}, while the rotational constant of free CO is $B=1.92$ cm^{-1}.

Rather than by saying that the vectors $\boldsymbol{r}$ and $\boldsymbol{R}$ rotate simultaneously, one may also explain this change of rota-

TABLE V. Band origin ΔE, effective rotational constant B, l-type doubling constant q, average position $\langle R\rangle$ of the CO mass center and vibrational amplitude ΔR for each ladder. The values of $\langle R\rangle$ and ΔR refer to the lowest states; the variations of $\langle R\rangle$ and ΔR within the ladders are very small, of the order of 0.001 Å for $\lambda\leqslant 7$.

Ladder	ΔE (cm^{-1})	$B(q)$ (cm^{-1})	$\langle R\rangle$ (Å)	ΔR (Å)
1 ($\Sigma,\sigma=+$)	0.0	1.73	0.211	0.052
2,3($\Pi,\sigma=\pm$)[a]	162.2	1.73(−0.18)	0.228	0.051
4 ($\Sigma,\sigma=+$)[b]	209.3	1.98	0.219	0.088
5 ($\Sigma,\sigma=+$)[c]	326.6	1.64	0.242	0.055
6,7($\Delta,\sigma=\pm$)[c]	324.8	1.64(−0.03)	0.242	0.050

[a]Libration fundamental.
[b]Radial stretch fundamental.
[c]Libration overtone.

tional constant by assuming that CO does not rotate about its center of mass, but about its "geometric center" (see Sec. II B). If we locate this center at a distance d from the center of mass, in the direction towards the C-atom, we can calculate from the increase by $(m_C+m_O)d^2$ in the moment of inertia, which corresponds to the change in B from 1.92 to 1.73 cm^{-1}, that $d=0.189$ Å. This is very close to the value of $R_{eq}=0.192$ Å obtained in Sec. II B, which is the distance between the center of mass of CO and its "geometric center." Also the average position of the CO center of mass, which for the ground state is $\langle R\rangle=0.211$ Å, is consistent with this idea. Hence, we may conclude that the lowest rotational ladder is caused by the rotation of CO, not about its center of mass, but about its "geometric center." It is forced to do so by the hard walls, i.e., the steep repulsive potential inside the C_{60} cage. Since this cage is nearly spherical, one observes a rotational structure similar to that of free CO. One must remember, however, that the "geometric center," which may now be understood as the origin about which the CO molecule effectively rotates inside C_{60}, is not a precisely defined quantity.

The second basic feature of the levels from the five-dimensional calculations with the full icosahedral C_{60} potential is the "crystal field" splitting of the $(2\lambda+1)$-fold degenerate levels calculated with the $\Lambda=0$ potential. The first terms in the expansion of the potential that represent the "corrugation" of the sphere are the terms with $\Lambda=6$. We find that these terms are small, only about 0.5% of the terms with $\Lambda=0$. It is therefore natural that the crystal field splittings are small too, but they are still of the order of a few cm^{-1}. It follows from the $SO(3)\supset I$ subduction rules in Table III that there is no splitting yet for $\lambda=0$, 1 and 2, that the $\lambda=3$ and $\lambda=4$ levels split into two sets of degenerate levels, T_2+G and $G+H$, respectively, the $\lambda=5$ levels into three sets, T_1+T_2+H, etc., see Table IV.

The third feature that characterizes the levels of $CO@C_{60}$ is that the origins of the different ladders are separated by large energy gaps. The second and third ladders are intriguing. Both start at $\lambda=1$. When we climb a given ladder we find rungs of alternating parity $L+j$. Thus we may characterize the parity σ of a whole ladder by writing the parity (g/u) of its rungs as $\sigma(-1)^{\lambda}$. Doing this, we find that the second ladder has $(+)$ parity and the third one $(-)$ parity. Note incidentally that the first and fourth ladders start with $\lambda=0$, which implies that their lowest levels contain basis functions with $L=j$. Hence these lowest levels must have g parity and, therefore, the parity of these ladders must be $\sigma=(+)$.

The level structure of the ladders 2 and 3 can be understood by comparison with the rovibrational levels of a linear triatomic molecule.[34] In its twofold degenerate excited bending states such a molecule carries a vibrational angular momentum $\pm l$. The rovibrational states associated with these bending vibrations have total angular momentum $J\geqslant l$ and their energies can be arranged in two ladders with rungs of alternating parity. The parity of these two ladders is opposite. They have a common origin and their rotational levels can be jointly fitted to the expression $\Delta E+B[J(J+1)-l^2]+qJ(J+1)$, where ΔE is the vibrational excitation energy, B is the unperturbed rotational constant, and q is the l-type doubling constant. The origin of this l-type doubling (or q-splitting) is the Coriolis coupling between the vibrational angular momentum and the overall rotation. Since only levels of equal parity and equal angular momentum J couple to one another, an $l=0$ ladder of given $(+/-)$ parity will affect only one of the two degenerate ladders, while the other one remains unperturbed (with $q=0$). This is precisely the pattern that we find for the ladders 2 and 3 (in calculations with $\Lambda=0$), if we associate the total angular momentum J with the quantum number λ and assume that the vibrational state is the bending fundamental of the "triatomic" with $l=1$ (a Π state). We may fit the levels in these two ladders to the expression $\Delta E+B[\lambda(\lambda+1)-l^2]+q\lambda(\lambda+1)$, with $q=0$ for ladder 3, because there are no $l=0$ ladders with parity $\sigma=(-)$. We then find that they have indeed a common origin $\Delta E=162.2$ cm^{-1} above the ground state level. The values of B and q are given in Table V. The value of B and the vibrational amplitude ΔR in the radial direction are practically the same as in the ground state ladder 1.

The question then arises: what is the (fundamental) bending vibration in this system? This question can be answered if we remember that at equilibrium the center of mass of CO is not in the center of the C_{60} sphere, but at $R=0.192$ Å, while the CO orientation vector $\boldsymbol{r}$ is antiparallel to the position vector $\boldsymbol{R}$. The simultaneous rotation of $\boldsymbol{r}$ and $\boldsymbol{R}$ is nearly unhindered, see Fig. 1, but if $\boldsymbol{r}$ and $\boldsymbol{R}$ change their relative orientation they meet a very steep energy barrier, see Fig. 2. So here we have our "linear triatomic" X–Y–Z with the X–Y bond given by $\boldsymbol{r}$ and the Y–Z bond by $\boldsymbol{R}$. The latter is not a chemical bond, of course, but the hard inner walls of C_{60} make the energy rise steeply when $\boldsymbol{r}$ and $\boldsymbol{R}$ move away from their linear (antiparallel) equilibrium orientation. This picture agrees with the observation that the average position $\langle R\rangle$ for the ladders 2 and 3 is further away from the center of the sphere, see Table V, than in the ground state ladder or even in the radially excited ladder 4. If the CO molecule is bent away from the radial vector $\boldsymbol{R}$ it may come closer to the inner wall of the sphere. Since this motion of the CO molecule inside C_{60} is a (strongly) hindered rotation rather than the bending of a linear triatomic, one should rather call the "bending" vibration a librational mode in this case.

In agreement with this interpretation of the ladders 2 and 3 is that we find three more ladders, not shown in Table IV, one of which starts with $\lambda=0$ and two with $\lambda=2$. These must be associated with the first overtone of the (Π state) libration fundamental, which has one component with $l=0$ (a Σ state) and one component with $l=2$ (a Δ state with vibrational angular momentum ±2). We may jointly fit the ladders 6 and 7 that correspond with the Δ state to the same expression as the ladders 2 and 3, which shows that these ladders indeed have a common origin at $\Delta E=324.8$ cm^{-1}. The origin of the (Σ state) ladder 5 is at $\Delta E=326.6$ cm^{-1}. The fact that these origins are not far apart and at almost twice the fundamental frequency of 162.2 cm^{-1} shows that the librational mode is nearly harmonic. The effective rotational and l-type doubling constants B and q, as well as the

information about the radial motion in these overtone states, are included in Table V. Also consistent with the interpretation of the libration as an $\boldsymbol{r}$ "bending" mode is that the average position $\langle R \rangle$ for the overtone is even closer to the inner wall of the sphere than for the libration fundamental, while the radial amplitude ΔR has not increased. The fundamental frequency of 162 cm^{-1}may be compared with the librational frequency of 194 cm^{-1} obtained in Ref. 12 from a harmonic analysis of the $CO@C_{60}$ potential provided by *ab initio* Hartree–Fock calculations.

The fourth ladder starts with $\lambda=0$, just as the lowest ladder, and it is easily seen that this fourth ladder corresponds to the first radially excited state ($n=1$) of the CO center of mass motion in the C_{60} cage. The average position $\langle R \rangle$ (see Table V) is not very different from the ground state (the lowest ladder), which can be understood if one realizes that $\langle R \rangle$ is mainly determined by the position of the "geometric center" of the CO molecule (as discussed above). The amplitude ΔR increases by nearly a factor of $\sqrt{3}$ when going from $n=0$ to $n=1$, as it should for a harmonic oscillator. We noticed already in our discussion of the results from the one-dimensional radial calculations that the radial potential is nearly harmonic. The radial excitation energy, i.e., the energy difference between the origins of the fourth and the lowest ladder, is 209.3 cm^{-1}. It is remarkable that the radial excitation energy from the one-dimensional calculations with all angles fixed at their equilibrium values (206.8 cm^{-1}) is very close to this value. This is another indication of the separability of this problem, provided that one defines the appropriate center about which the CO molecule is forced to rotate. A one-dimensional calculation with the isotropic ($L_1=L_2=\Lambda=M_\Lambda=0$) term in the potential, which would correspond to the free rotation of CO about its center of mass, gives a very different radial excitation energy.

The rotational constant B that can be extracted from the levels in ladder 4 is much larger than for all other ladders and even larger than the rotational constant of free CO. Most of this increase of B can be explained by the same mechanism that causes the l-type doubling of the ladders 2 and 3. Ladder 4 of parity $\sigma=(+)$ interacts with the nearby ladder 2 of the same parity by Coriolis coupling. This gives a downward shift of the rotational constant for the lower ladder 2, which for this Π-state is reflected by the large negative value of the l-type doubling constant $q=-0.18$ cm^{-1}. The upper (Σ-state) ladder 4 must have a corresponding upward shift of its B value by approximately the same amount. This explains the largest part of the difference between the value of $B=1.98$ cm^{-1} of ladder 4 and the ground state value $B=1.73$ cm^{-1}. The remaining part may be due to a small shift of the "geometric center" of CO by the radial excitation.

In Table VI we list the energies for the free form of $CO@C_{60}$ with $J=K=0$. As might be expected there are only minor differences with the energies of $CO@C_{60}$ in the solid form, since the only changes in the Hamiltonian for $J=0$ are the appearance of the reduced mass μ_{AB}, instead of the mass of CO, and the additional term $\boldsymbol{\lambda}^T\mathbb{I}^{-1}\boldsymbol{\lambda}$. The latter term is very small because the principal moments of inertia of C_{60} are 6065 amu Å^2 and its rotational constants are only 0.0028 cm^{-1}. The upward shift of the energy levels is mainly due to the reduction of the effective mass. Of course, there will also be rotational levels for different values of J and K, and one must include the Coriolis coupling associated with the cross terms $2\boldsymbol{\lambda}^T\mathbb{I}^{-1}\boldsymbol{J}$ in the Hamiltonian, if non-zero J states are considered.

TABLE VI. Energy levels (in cm^{-1}) of the freely rotating complex $CO@C_{60}$ for $J=K=0$.

λ	irrep				
	Ladder	1(+)	2(+)	3(−)	4(+)
0	A	−805.06			−591.61
1	T_1	−801.59	−638.76	−638.32	−587.47
2	H	−794.68	−632.70	−631.40	−579.83
3	G	−785.00	−623.81	−620.41	−568.83
	T_2	−783.27	−623.22	−621.78	−566.87
4	G	−771.11	−610.70	−607.11	−552.52
	H	−769.70	−610.43	−606.80	−550.97
5	T_2	−753.33	−593.18	−589.09	−529.81
	H	−752.91	−592.82	−589.00	−529.39
	T_1	−751.68	−592.27	−588.85	−528.11
6	G	−730.84	−568.43	−565.51	−498.10
	H	−730.38	−568.02	−565.42	−497.63
	T_1	−729.54	−567.32	−565.11	−496.74
	A	−728.82	−566.69	−564.91	−496.02
7	G	−700.48	−534.32	−532.69	−453.05
	T_2	−700.28	−534.22	−532.62	−452.88
	H	−699.72	−533.63	−532.35	−452.33
	T_1	−698.78	−532.65	−531.93	−451.45
8	H	−657.20	−486.69	−485.38	−392.15
	T_2	−656.80	−486.28	−485.16	−391.72
	G	−656.60	−486.05	−485.06	−391.43
	H	−655.64	−485.03	−484.53	−390.68
9	T_1	−596.70	−416.24	−420.24	
	H	−596.32	−415.94	−420.04	
	G	−596.07	−415.73	−419.90	
	G	−595.05	−414.65	−419.29	
	T_2	−595.01	−414.61	−419.26	

B. Infrared spectrum

In Table VII we list the line strengths [or transition probabilities, see Eq. (35)] for transitions that start from the levels lower than 25 cm^{-1}, i.e., the levels in ladder 1 with $\lambda \leqslant 3$. If L and j were good quantum numbers, the dipole moment given in Eq. (33) would lead to the selection rules $\Delta L=0$ and $\Delta j=\pm 1$, since it does not depend on $\boldsymbol{R}$ and it depends on the orientation of $\boldsymbol{r}$ in the same way as the dipole moment of the CO monomer. This is not at all true, however, basis functions with different L and j are strongly mixed in the eigenvectors. Instead we find the selection rules $\Delta\lambda=0$ or ± 1. Although λ is not an exact quantum number either, all transitions which do not obey these selection rules are weaker by several orders of magnitude than those shown in Table VII. This is consistent with the observation in Sec. IV A that the energy levels are ordered in rotational ladders, with the rungs numbered by λ.

The strongest transitions are those within ladder 1, which obey the selection rules $\Delta\lambda=\pm 1$. They correspond to

TABLE VII. Line strengths in units μ_T^2, where μ_T is the dipole or the transition dipole μ^{01} of free CO. Only $|\Delta\lambda| \leqslant 1$ transitions are listed.

irrep(λ) → irrep′(λ')	E_i (cm^{-1})	E_f (cm^{-1})	ΔE (cm^{-1})	Line strength
$\Delta\lambda=1$ within ladder 1				
$A_g(0)\rightarrow T_{1u}(1)$	−809.81	−806.37	3.44	0.9974
$T_{1u}(1)\rightarrow H_g(2)$	−806.37	−799.49	6.88	1.9941
$H_g(2)\rightarrow G_u(3)$	−799.49	−789.86	9.63	1.8122
$H_g(2)\rightarrow T_{2u}(3)$	−799.49	−788.13	11.36	1.1800
$T_{2u}(3)\rightarrow G_g(4)$	−788.13	−776.05	12.08	0.4971
$T_{2u}(3)\rightarrow H_g(4)$	−788.13	−774.64	13.49	1.3147
$G_u(3)\rightarrow G_g(4)$	−789.86	−776.05	13.81	1.3296
$G_u(3)\rightarrow H_g(4)$	−789.86	−774.64	15.22	0.8476
$\Delta\lambda=-1$ from ladder 1 to ladder 2				
$T_{2u}(3)\rightarrow H_g(2)$	−788.13	−640.32	147.81	1.07×10^{-3}
$G_u(3)\rightarrow H_g(2)$	−789.86	−640.32	149.54	1.49×10^{-3}
$H_g(2)\rightarrow T_{1u}(1)$	−799.49	−646.34	153.15	1.25×10^{-3}
$\Delta\lambda=0$ from ladder 1 to ladder 3				
$T_{1u}(1)\rightarrow T_{1g}(1)$	−806.37	−645.89	160.48	3.71×10^{-3}
$H_g(2)\rightarrow H_u(2)$	−799.49	−639.00	160.49	6.19×10^{-3}
$T_{2u}(3)\rightarrow G_g(3)$	−788.13	−628.07	160.07	3.44×10^{-3}
$G_u(3)\rightarrow T_{2g}(3)$	−789.86	−629.44	160.42	3.75×10^{-3}
$G_u(3)\rightarrow G_g(3)$	−789.86	−628.07	161.80	1.52×10^{-3}
$\Delta\lambda=1$ from ladder 1 to ladder 2				
$A_g(0)\rightarrow T_{1u}(1)$	−809.81	−646.34	163.47	2.46×10^{-3}
$T_{1u}(1)\rightarrow H_g(2)$	−806.37	−640.32	166.05	3.69×10^{-3}
$H_g(2)\rightarrow T_{2u}(3)$	−799.49	−631.50	167.99	2.23×10^{-3}
$H_g(2)\rightarrow G_u(3)$	−799.49	−630.90	168.59	2.71×10^{-3}
$T_{2u}(3)\rightarrow G_g(4)$	−788.13	−618.46	169.67	0.95×10^{-3}
$T_{2u}(3)\rightarrow H_g(4)$	−788.13	−618.19	169.94	2.19×10^{-3}
$G_u(3)\rightarrow G_g(4)$	−789.86	−618.46	171.40	1.87×10^{-3}
$G_u(3)\rightarrow H_g(4)$	−789.86	−618.19	171.67	1.47×10^{-3}
$\Delta\lambda=-1$ from ladder 1 to ladder 4				
$T_{2u}(3)\rightarrow H_g(2)$	−788.13	−588.75	199.38	8.90×10^{-6}
$G_u(3)\rightarrow H_g(2)$	−789.86	−588.75	201.11	1.67×10^{-6}
$H_g(2)\rightarrow T_{1u}(1)$	−799.49	−596.33	203.16	0.03×10^{-6}
$T_{1u}(1)\rightarrow A_g(0)$	−806.37	−600.49	205.87	1.03×10^{-6}
$\Delta\lambda=1$ from ladder 1 to ladder 4				
$A_g(0)\rightarrow T_{1u}(1)$	−809.81	−596.33	213.48	1.24×10^{-5}
$T_{1u}(1)\rightarrow H_g(2)$	−806.37	−588.75	217.62	4.69×10^{-5}
$H_g(2)\rightarrow G_u(3)$	−799.49	−577.77	221.72	6.28×10^{-5}
$H_g(2)\rightarrow T_{2u}(3)$	−799.49	−575.83	223.66	4.46×10^{-5}
$T_{2u}(3)\rightarrow G_g(4)$	−788.13	−561.51	226.62	2.85×10^{-5}
$T_{2u}(3)\rightarrow H_g(4)$	−788.13	−559.97	228.17	8.32×10^{-5}
$G_u(3)\rightarrow G_g(4)$	−789.86	−561.51	228.35	8.68×10^{-5}
$G_u(3)\rightarrow H_g(4)$	−789.86	−559.97	229.90	5.91×10^{-5}

the pure rotational spectrum of CO or, if the CO stretch vibration is excited, to the rotational P and R branches of the fundamental stretch band in the infrared spectrum. Note, however, that the rotational constant B associated with these transitions in $CO@C_{60}$ is significantly different from that of free CO, since CO cannot rotate freely about its center of mass, but only about its "geometric center." Moreover, one may directly read from Table VII that the lines which involve levels with $\lambda \geqslant 3$ are split because C_{60} is not spherical but icosahedral. The associated "crystal field" splittings are of the order of a few cm^{-1}, i.e., of the same magnitude as the rotational splittings. Hence, they should be visible even in a low resolution spectrum. If we add up the transition probabilities between the levels that correspond to the same initial λ and final λ', we obtain very nearly the line strengths of free CO: 1 for the $0\rightarrow1$ transition, 2 for the $1\rightarrow2$ transition, 3 for the $2\rightarrow3$ transition, and 4 for the $3\rightarrow4$ transition.

The transitions from ladder 1 to the next higher ladders 2 and 3 have considerably smaller line strength, but given that the infrared absorption intensity contains the excitation frequency [see Eq. (36)] which is here about 50 times larger than the rotational spacings, they may still be observable. As explained in Sec. IV A, the ladders 2 and 3 represent a librationally excited state. The excitations to this state must obey the (approximate) selection rules $\Delta\lambda=0$ or ±1. It is obvious that for parity reasons the P and R type transitions with $\Delta\lambda=\pm1$ must have their final states in ladder 2, while the Q type transitions with $\Delta\lambda=0$ must end in ladder 3. The rovibrational structure of ladders 2 and 3 could be interpreted as that of a linear triatomic molecule in a Π-bending state. Another parallel with this system[34] is that the Q type transitions are even somewhat stronger than the P and R type transitions. The position of the Q band relative to that of the P and R bands reflects the q-splitting between the ladders 2 and 3. This makes the spectrum in the region around 160 cm^{-1} very different from the spectrum of free CO. Finally we observe that the "crystal field" splittings in all these transitions, just as in the pure rotational transitions, are of the same order of magnitude as the rotational splittings. This further breaks the regularity of the rovibrational spectrum.

The last series of line strengths presented in Table VII regards the transitions to the radially excited states in ladder 4, with excitation energies around 210 cm^{-1}. These obey the same $\Delta\lambda=\pm1$ selection rules as the purely rotational transitions within ladder 1, but they are weaker again by two orders of magnitude than the librational transitions discussed in the preceding paragraph. The reason why the radial excitation does not lead to a substantial transition dipole moment is that the dipole operator does not depend on the radial coordinate, cf. Eq. (33). The remaining very small values are due to the imperfect separation between the radial and angular motions. The transitions to the librational overtone states in the ladders 5, 6 and 7 are not even listed in Table VII, because they are very weak too.

In Fig. 4 we show the far-infrared spectrum at a temperature of 77 K calculated by means of Eq. (36). Initial states up to 500 cm^{-1} above the ground state were included in this calculation. The strong lines below 100 cm^{-1} originate from the "perturbed rotational" transitions within ladder 1. Especially in the $R(2)$, $R(3)$ and $R(4)$ lines the crystal field splittings are clearly visible. The weaker lines to the right of the $R(5)$, $R(6)$, $R(7)$ and $R(8)$ lines are the corresponding R lines of a hot band which originates from the transitions within the librationally excited ladders 2 and 3. The librational band around 160 cm^{-1}, although weaker than the rotational band, is clearly observable. It has a P branch starting at $P(2)$, a Q branch starting at $Q(1)$, and an R branch starting at $R(0)$. Also here the crystal field splittings are visible especially in the $P(3)$, $P(4)$, $P(5)$, $R(2)$, $R(3)$, and $R(4)$ lines. The P and R lines become relatively strong for

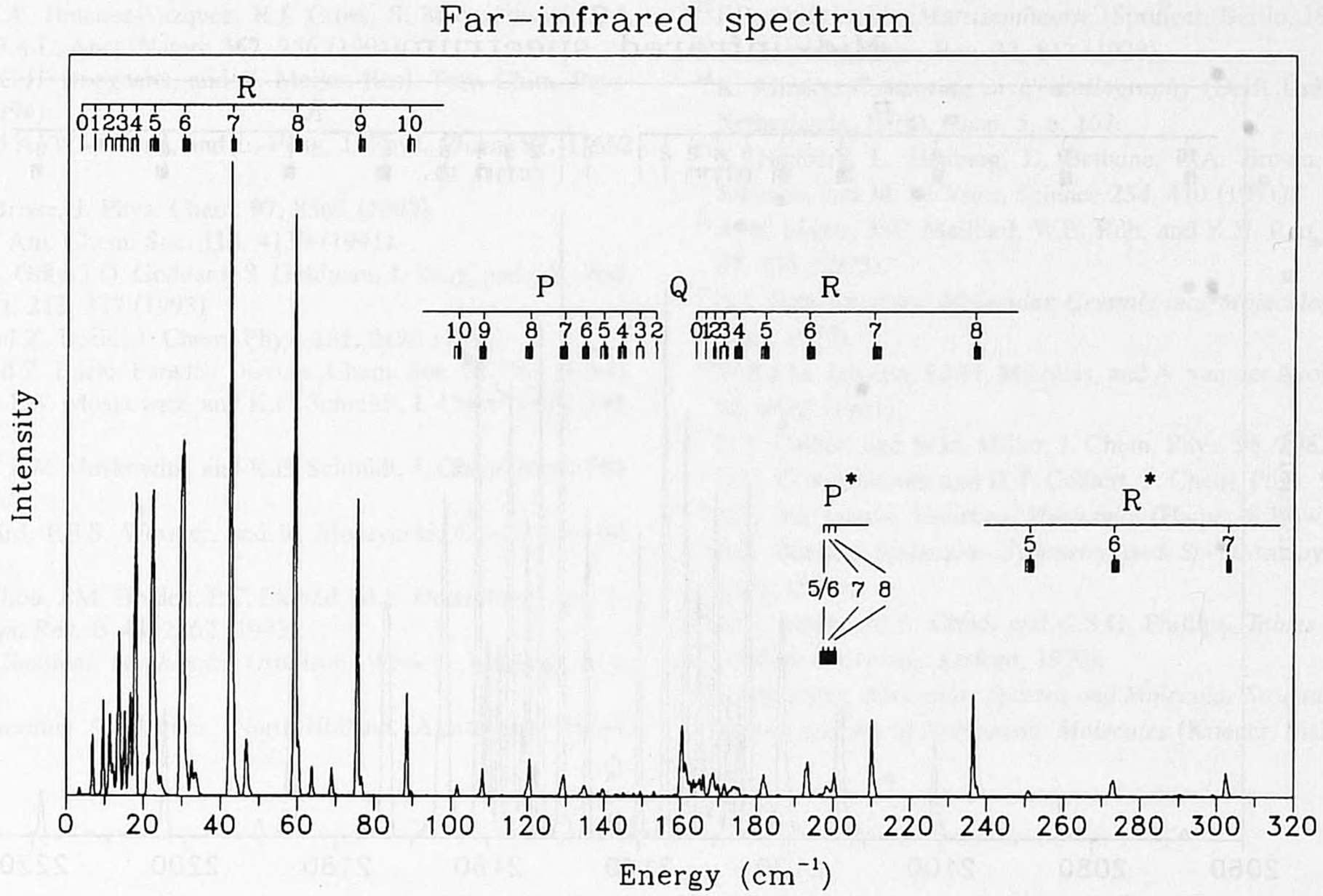

FIG. 4. Calculated far-infrared absorption spectrum at 77 K. A Gaussian line shape is assumed, full width at half maximum 0.5 cm^{-1}. The P and R branches marked with an asterisk (*) belong to the radial excitation band with origin 209.3 cm^{-1}. The vertical bars that contain the labels of the lines mark the frequencies from the calculations with the $\Lambda=0$ potential. The icosahedral field splittings are indicated by the vertical bars below the labels (transitions with intensities less than 10% of the strongest ones are omitted).

higher values of λ because the librationally excited Π states in the even parity ladder 2, which are the final states in these P and R transitions, mix with the ground Σ states by Coriolis coupling (the same mechanism that leads to the l-type doubling of the ladders 2 and 3, see Sec. IV A, although the latter effect is dominated by the mixing between the ladders 2 and 4). Since the (rotational) transition strengths between the ground state levels are very large, even a small amount of mixing of the ground state into the librationally excited state will considerably raise the intensities in the fundamental libration band. Even the radial excitation band (origin 209.3 cm^{-1}) can be seen. It has a $P(5)/P(6)$ band head at 197 cm^{-1} and some R lines that are sufficiently strong to be observable.

In Fig. 5 we present the mid-infrared spectrum that accompanies the excitation of the CO fundamental stretch vibration. The relative intensities of the lines are different, because the excited state is not populated in this case and because the CO fundamental stretch excitation energy (2143.27 cm^{-1}) has to be included in the factor (E_f-E_i) in the intensity formula. As a result, the librational band becomes relatively very weak and we show only the perturbed rotational band, with its P and R branches. To the right of the $R(5)$, $R(6)$, $R(7)$ and $R(8)$ lines and to the left of the $P(6)$, $P(7)$, $P(8)$ and $P(9)$ lines one observes again the corresponding hot band lines originating from the transitions within the ladders 2 and 3. Note that the hot band transitions within these librationally excited ladders give also rise to a Q band which is clearly observable.

V. SUMMARY AND CONCLUSIONS

After deriving a Hamiltonian for CO@C_{60} and similar endohedral complexes, we have calculated the energy levels and wave functions corresponding to the rotations and vibrations of CO in C_{60}, from an atom–atom model potential. This potential and the wave functions were expanded in a coupled free rotor basis for the angular coordinates, adapted to the icosahedral symmetry of C_{60}. For the radial coordinate we used a discrete variable representation. Although the calculated eigenstates are not separable (in the coordinates used or in any other set of Jacobi coordinates) and the quantum numbers j and L that correspond to the rotation of CO (about its center of mass) and the rotation of its position vector $\boldsymbol{R}$ are strongly mixed, the calculated level structure can be understood from three basic features:

(1) Simultaneous rotations of CO (the vector $\boldsymbol{r}$) and its position vector $\boldsymbol{R}$ inside the nearly spherical C_{60}. The corresponding quantum number λ numbers the rungs of various rotational ladders. The rotational constants associated with these ladders are rather different and differ also from the value for free CO. The lowest ladder can also be understood as a rotation of CO about its "geometric center," to which it is forced by the hard inner walls of the C_{60} cage.
(2) The splittings of these rotational levels due to the asphericity of C_{60}. These "crystal field" splittings are of the

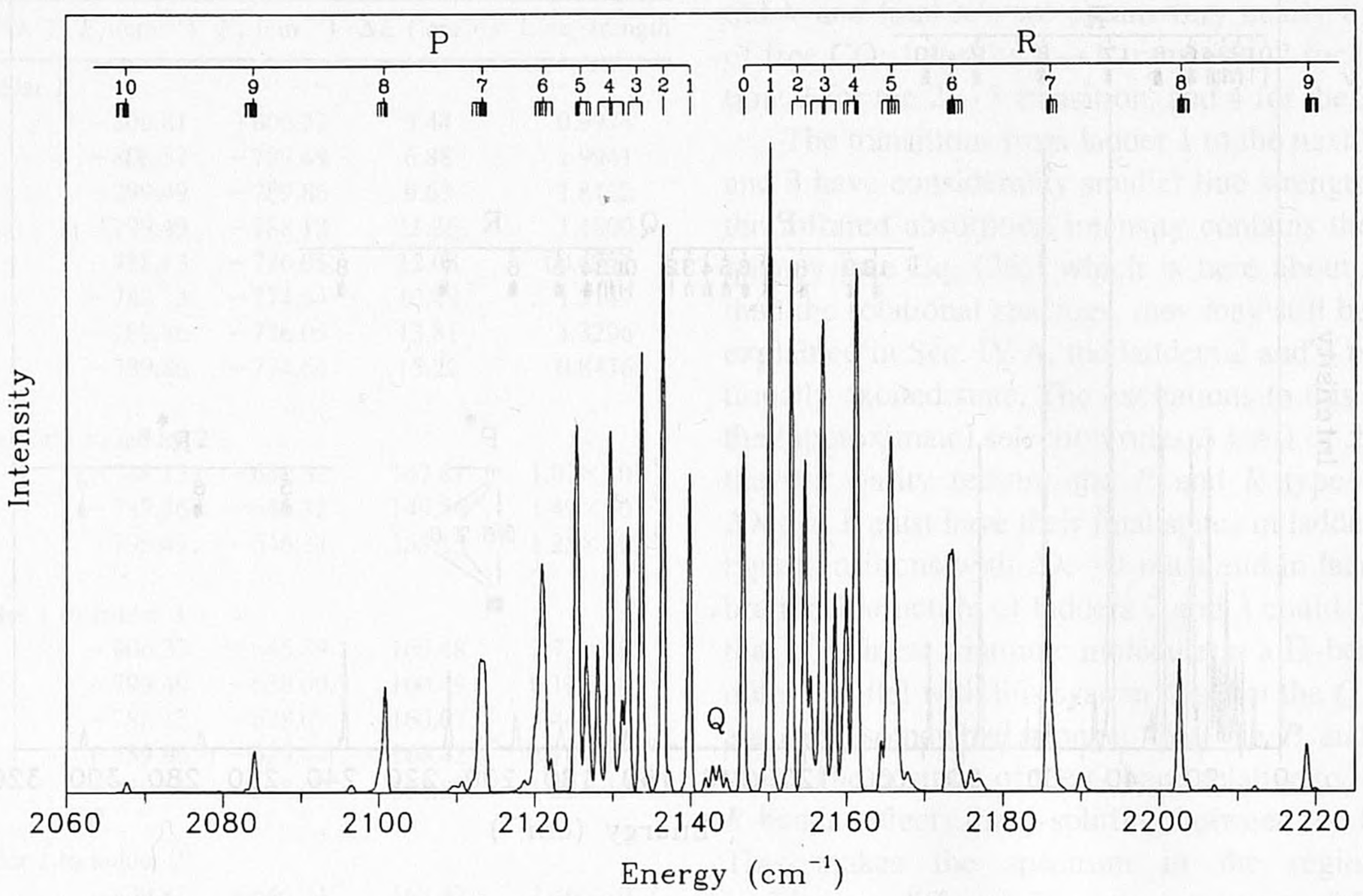

FIG. 5. Calculated mid-infrared absorption spectrum at 77 K; the CO fundamental stretch frequency is 2143.27 cm^{-1}. For details, see the caption of Fig. 4.

same order of magnitude as the rotational spacings and they obey the rules of the icosahedral I_h symmetry group.

(3) Vibrations of CO against the hard inner walls of C_{60}. The first radial excitation energy is 209 cm^{-1}, the twofold degenerate libration has a fundamental frequency of 162 cm^{-1}. These vibrations are nearly harmonic and they determine the large offsets of the different rotational ladders. The fundamental libration, which may be understood as a bending vibration of $\boldsymbol{r}$ and $\boldsymbol{R}$ with respect to the linear (antiparallel) equilibrium orientation, gives a rovibrational level structure very similar to that of a linear triatomic molecule in a Π-bending state. This explains the fact that the corresponding rovibrational ladders start at $\lambda=1$, as well as the q-splitting between these ladders. Librational overtone states have been found too: a Σ state at 327 cm^{-1} and a (q-split) Δ state at 325 cm^{-1}.

We have calculated the eigenstates of CO@C_{60} fixed (in a solid), as well as those of the freely rotating complex (in the gas phase or in a molecular beam). The levels of the free complex with $J=0$ are just slightly shifted upwards, with respect to those of CO in fixed C_{60}. This is mainly caused by the difference between the reduced mass of the complex and the mass of the CO monomer.

The selection rules for infrared transitions between these levels are given, and the line strengths of the allowed transitions are quantitatively calculated. In a predicted infrared spectrum (at 77 K) it can be seen that the "perturbed rotational" band is the strongest, but that also the librational band has sufficient intensity to be observable and that even the radial excitation band may be seen. The rotational band and the radial excitation band have only P and R branches, just as the rovibrational bands of free CO, but the librational band has also a Q branch (just as the $\Sigma\rightarrow\Pi$-bending transitions in a linear triatomic molecule). The frequency of the libration, the rotational and q-splitting constants, and the icosahedral symmetry splittings of the rovibrational bands are very sensitive probes of the intermolecular potential of CO in C_{60}. If these quantities will be measured, we will probably be able to improve the atom-atom model potential used in the present calculations.

ACKNOWLEDGMENTS

We thank Dr. Gerrit Groenenboom for his assistance with the implementation of the DVR algorithm, Professor Gerard Meijer for stimulating discussions and for a number of very useful comments on the manuscript.

[1] H.R. Kroto, J.R. Heath, S.C. O'Brien, R.F. Curl, and R.E. Smalley, Nature **318**, 162 (1985).
[2] T. Weiske, J. Hrušák, D.K. Böhme, and H. Schwartz, Chem. Phys. Lett. **186**, 459 (1991).
[3] Z. Wan, J.F. Christian, and S.L. Anderson, J. Chem. Phys. **96**, 3344 (1992).
[4] G. Meijer (private communication).
[5] L.S. Wang, J.M. Alford, Y. Chai, M. Diener, J. Zhang, S.M. McClure, T. Guo, G.E. Scuseria, and R.E. Smalley, Chem. Phys. Lett. **207**, 354 (1993).
[6] J.R. Heath, S.C. O'Brien, Q. Zhang, Y. Liu, R.F. Curl, H.W. Kroto, F.K. Tittel, and R.E. Smalley, J. Am. Chem. Soc. **107**, 7779 (1985).
[7] D.S. Bethune, M.S. de Vries, R.D. Johnson, J.R. Salem, and C.S. Yannoni, Nature **366**, 123 (1993).

[8] M. Saunders, H.A. Jimenez-Vazquez, R.J. Cross, S. Mroczkowski, D.I. Freedberg, and F.A.L. Anet, Nature **367**, 256 (1994).
[9] I. Holleman, M.G.H. Boogaarts, and G. Meijer, Recl. Trav. Chim. Pays-Bas **113**, 543 (1994).
[10] C.I. Williams, M.A. Whitehead, and L. Pang, J. Phys. Chem. **97**, 11652 (1993).
[11] L. Pang and F. Brisse, J. Phys. Chem. **97**, 8562 (1993).
[12] J. Cioslowski, J. Am. Chem. Soc. **113**, 4139 (1991).
[13] C.G. Joslin, C.G. Gray, J.D. Goddard, S. Goldman, J. Yang, and J.D. Poll, Chem. Phys. Lett. **213**, 377 (1993).
[14] M. Mandziuk and Z. Bačić, J. Chem. Phys. **101**, 2126 (1994).
[15] M. Mandziuk and Z. Bačić, Faraday Discuss. Chem. Soc. **97**, 265 (1994).
[16] S. Liu, Z. Bačić, J.W. Moskowitz, and K.E. Schmidt, J. Chem. Phys. **101**, 6359 (1994).
[17] S. Liu, Z. Bačić, J.W. Moskowitz, and K.E. Schmidt, J. Chem. Phys. **103**, 1829 (1995).
[18] A. van der Avoird, P.E.S. Wormer, and R. Moszynski, Chem. Rev. **94**, 1931 (1994).
[19] Z.-H. Dong, P. Zhou, J.M. Holden, P.C. Eklund, M.S. Dresselhaus, and G. Dresselhaus, Phys. Rev. B **48**, 2862 (1993).
[20] H. Goldstein, *Classical Mechanics* (Addison–Wesley, Reading, MA, 1980), 2nd ed.
[21] A. Messiah, *Quantum Mechanics* (North-Holland, Amsterdam, 1969), Vol. I.
[22] F.R. Gantmacher, *Matrizentheorie* (Springer, Berlin, 1986).
[23] B. Podolsky, Phys. Rev. **32**, 812 (1928).
[24] K. Mirsky, *Computing in Cristallography* (Delft University, Delft, The Netherlands, 1978), Chap. 5, p. 167.
[25] K. Hedberg, L. Hedberg, D. Bethune, C.A. Brown, H.C. Dorn, R.D. Johnson, and M. de Vries, Science **254**, 410 (1991).
[26] A.W. Mantz, J.-P. Maillard, W.B. Roh, and K.N. Rao, J. Mol. Spectrosc. **57**, 155 (1975).
[27] A.I. Kitaigorodsky, *Molecular Crystals and Molecules* (Academic, New York, 1973).
[28] W.B.J.M. Janssen, J.J.M. Michiels, and A. van der Avoird, J. Chem. Phys. **94**, 8402 (1991).
[29] D.T. Colbert and W.H. Miller, J. Chem. Phys. **96**, 1982 (1992).
[30] G.C. Groenenboom and D.T. Colbert, J. Chem. Phys. **99**, 9681 (1993).
[31] D.A. McQuarrie, *Statistical Mechanics* (Harper & Row, New York, 1976).
[32] P.R. Bunker, *Molecular Symmetry and Spectroscopy* (Academic, New York, 1979).
[33] P.W. Atkins, M.S. Child, and C.S.G. Phillips, *Tables for Group Theory* (Oxford University, Oxford, 1970).
[34] G. Herzberg, *Molecular Spectra and Molecular Structure, II. Infrared and Raman Spectra of Polyatomic Molecules* (Krieger, Malabar, 1991).